

CERN-EP-2022-290

20 December 2022

Azimuthal anisotropy of jet particles in p–Pb and Pb–Pb collisions at $\sqrt{s_{\text{NN}}} = 5.02 \text{ TeV}$

ALICE Collaboration*

Abstract

The azimuthal anisotropy of particles associated with jets (jet particles) at midrapidity is measured for the first time in p–Pb and Pb–Pb collisions at $\sqrt{s_{\text{NN}}} = 5.02 \text{ TeV}$ down to transverse momentum (p_T) of $0.5 \text{ GeV}/c$ and $2 \text{ GeV}/c$, respectively, with ALICE. The results obtained in p–Pb collisions are based on a novel three-particle correlation technique. The azimuthal anisotropy coefficient v_2 in high-multiplicity p–Pb collisions is positive, with a significance reaching 6.8σ at low p_T , and its magnitude is smaller than in semicentral Pb–Pb collisions. In contrast to the measurements in Pb–Pb collisions, the v_2 coefficient is also found independent of p_T within uncertainties. Comparisons with the inclusive charged-particle v_2 and with AMPT calculations are discussed. The predictions suggest that parton interactions play an important role in generating a non-zero jet-particle v_2 in p–Pb collisions, even though they overestimate the reported measurement. These observations shed new insights on the understanding of the origin of the collective behaviour of jet particles in small systems such as p–Pb collisions, and provide significant stringent new constraints to models.

*See Appendix A for the list of collaboration members

1 Introduction

The study of ultrarelativistic heavy-ion collisions aims to investigate the properties of strongly-interacting matter characterised by high energy density and temperature, known as the quark–gluon plasma (QGP) [1, 2]. In non-central collisions, the initial spatial anisotropy of the overlap region of the colliding nuclei is converted into an anisotropy in momentum space via interactions among the medium constituents. The final-state anisotropies are quantified by the coefficients (v_n) of a Fourier decomposition of the azimuthal (ϕ) distribution of produced particles [3, 4]:

$$\frac{d^2N}{dp_T d\phi} = \frac{1}{2\pi} \frac{dN}{dp_T} \left(1 + 2 \sum_{n=1}^{\infty} v_n(p_T) \cos[n(\phi - \Psi_n)] \right), \quad (1)$$

where p_T is the transverse momentum and Ψ_n is the azimuthal angle of the symmetry plane for the n^{th} harmonic. Measurements of the v_n coefficients are expected to provide information on the initial state and the transport properties of the produced medium. The dominant coefficient is the second Fourier coefficient v_2 , referred to as the elliptic flow [4, 5], which provides information on the collective expansion of the medium at low p_T [6] and the path-length dependence of medium-induced parton energy loss at high p_T [7, 8].

Collisions of small systems such as proton–nucleus are studied in detail to characterise the cold nuclear matter (CNM) effects which are also present in heavy-ion collisions, providing critical information for understanding QGP properties. These CNM effects influence parton distribution functions [9], induce Cronin-like effects [10], and cause energy loss [11]. As in heavy-ion collisions, a significant v_2 was observed in p–Pb collisions for soft as well as hard probes, such as open heavy-flavour hadrons [12, 13], quarkonia [14, 15], and high- p_T charged hadrons [16, 17]. A positive v_2 was also reported for charged particles [18–22] and muons from charm-hadron decays [23] in pp collisions, while the v_2 of muons from beauty-hadron decays was consistent with zero [23]. The observation of a non-zero v_2 in small collision systems raised the question whether small-size QGP droplets are formed in these conditions. However, the particle yields at high p_T in p–Pb collisions are found to be unmodified within uncertainties compared to the same measurements in pp collisions, scaled by the number of binary nucleon–nucleon collisions [17, 24–29]. Such an observation indicates that final-state effects are not significant in small collision systems. Therefore, alternative scenarios have been proposed, including color exchange in the final state [30], initial-state effects due to gluon saturation [31–33], or anisotropic escape of partons from the surface of the interaction zone [34].

This paper reports the first measurements of the p_T -differential v_2 of jet particles (particles associated with jets) at midrapidity in high-multiplicity p–Pb collisions and semicentral Pb–Pb collisions at $\sqrt{s_{\text{NN}}} = 5.02$ TeV with ALICE. The jet-particle v_2 measured down to lower p_T compared to the v_2 of reconstructed jets is of particular interest since it is clearly separated from particles from soft processes. These results are compared with inclusive charged-particle v_2 measurements in both p–Pb and Pb–Pb collisions, as well as with previous results of the v_2 of reconstructed jets in Pb–Pb collisions at $\sqrt{s_{\text{NN}}} = 2.76$ TeV [35]. Comparisons with A MultiPhase Transport (AMPT) model predictions [36, 37] are also discussed.

The article is organised as follows. Section 2 presents the ALICE apparatus with an emphasis on the detectors used in the analysis and the data taking conditions. The analysis strategy and the estimation of systematic uncertainties are described in Section 3. Section 4 presents the results for jet particles and inclusive charged particles measured in p–Pb and Pb–Pb collisions as well as comparisons with AMPT model calculations in p–Pb collisions. Concluding remarks are drawn in Section 5.

2 Experimental apparatus and data samples

The analysis is performed on the p–Pb and Pb–Pb data collected with the ALICE detector in 2016 and 2015, respectively. In p–Pb collisions, the asymmetry of the proton and Pb beam energies results in

a rapidity shift of the nucleon–nucleon centre-of-mass by 0.465 in the direction of the proton beam with respect to the laboratory frame. In the following, the pseudorapidity η values correspond to the laboratory frame. A detailed description of the detector and its performance is given in Refs. [38, 39]. The analysis is based on tracks reconstructed using the Time Projection Chamber (TPC) [40] located inside a large solenoidal magnet with a 0.5 T field parallel to the LHC beam direction and covering $|\eta| < 0.9$. Information from the Inner Tracking System (ITS) [41] is used to improve the spatial and momentum resolution of the reconstructed tracks. The Silicon Pixel Detector (SPD) [41, 42], comprising the two innermost layers of the ITS covering $|\eta| < 2.0$ and $|\eta| < 1.4$, is employed together with the TPC to determine the position of the primary interaction vertex. The Forward Multiplicity Detector (FMD) [43] consists of three sets of silicon strip sensors, covering $-3.5 < \eta < -1.7$ (FMD3) and $1.7 < \eta < 5$ (FMD1,2). The FMD is used in p–Pb collisions for the event selection and to extract the v_2 coefficient via long-range three-particle correlations. The V0 detector, formed by two scintillator arrays covering $-3.7 < \eta < -1.7$ (V0C) and $2.8 < \eta < 5.1$ (V0A), is used for triggering, event characterisation and centrality determination [44]. Two sets of Zero Degree Calorimeters (ZDC) [39], located at ± 112.5 m from the nominal interaction point along the beam line, are also used for the event selection.

The analysis of the p–Pb and Pb–Pb samples is based on events selected by a minimum bias (MB) trigger. The MB trigger is provided by the coincidence of signals in the two V0 scintillator arrays. Pile-up events are removed based on an event selection which uses the information from the V0 and SPD to tag events with multiple vertices. The beam-induced background is reduced offline by exploiting the V0 and ZDC timing information. In addition, in p–Pb collisions, the correlation between the multiplicity measured in the FMD and V0 is used to further remove contamination from beam-induced background and outliers in the FMD multiplicity distribution. Only events with a primary vertex along the beam axis, z_{vtx} , within ± 10 cm from the nominal interaction point are considered. About 526 million p–Pb and 60 million Pb–Pb events passed the event selection criteria. In Pb–Pb collisions, the centrality classes are defined as percentiles of the Pb–Pb hadronic cross section, and determined using the total energy deposited in the V0 arrays [45]. The p–Pb data sample is divided into several multiplicity classes based on the energy deposited in the V0A scintillators, located in the Pb-going direction [45]. In the p–Pb analysis, only the high-multiplicity class 0–10% and the low-multiplicity class 60–100% are studied. The measurements in Pb–Pb collisions are presented in the 20–60% centrality interval.

Reconstructed charged-particle tracks are selected by applying the standard conditions given in Refs. [46–48]. They concern the number of space points and the quality of the track fit in the TPC, and the distance of closest approach to the primary vertex. Tracks are selected with $p_T > 0.5$ GeV/c and $|\eta| < 0.8$ in both p–Pb and Pb–Pb collisions. Hits in the FMD are measured in the η regions limited to $-3.2 < \eta < -1.8$ and $1.8 < \eta < 4.8$.

3 Data analysis

The procedure developed to calculate the jet-particle v_2 is detailed in Ref. [48]. The jet-particle v_2 measurement consists of four main parts: i) construction of the two-particle (charged particles at midrapidity regarded as trigger and associated particles) correlation function, ii) extraction of the near-side jet peak (the signal) and background yields containing also the away-side jet yields, by fitting the two-particle correlation function, iii) calculation of the v_2 of particle pairs represented by the trigger particles using three-particle correlations in p–Pb collisions, for the first time, and the scalar product method with the three-subevent technique in Pb–Pb collisions, and iv) extraction of the v_2 of jet particles, in given trigger- and associated-particle p_T intervals, using a two-component fit function that takes into account the relative contribution from both jets and background to the particle-pair v_2 .

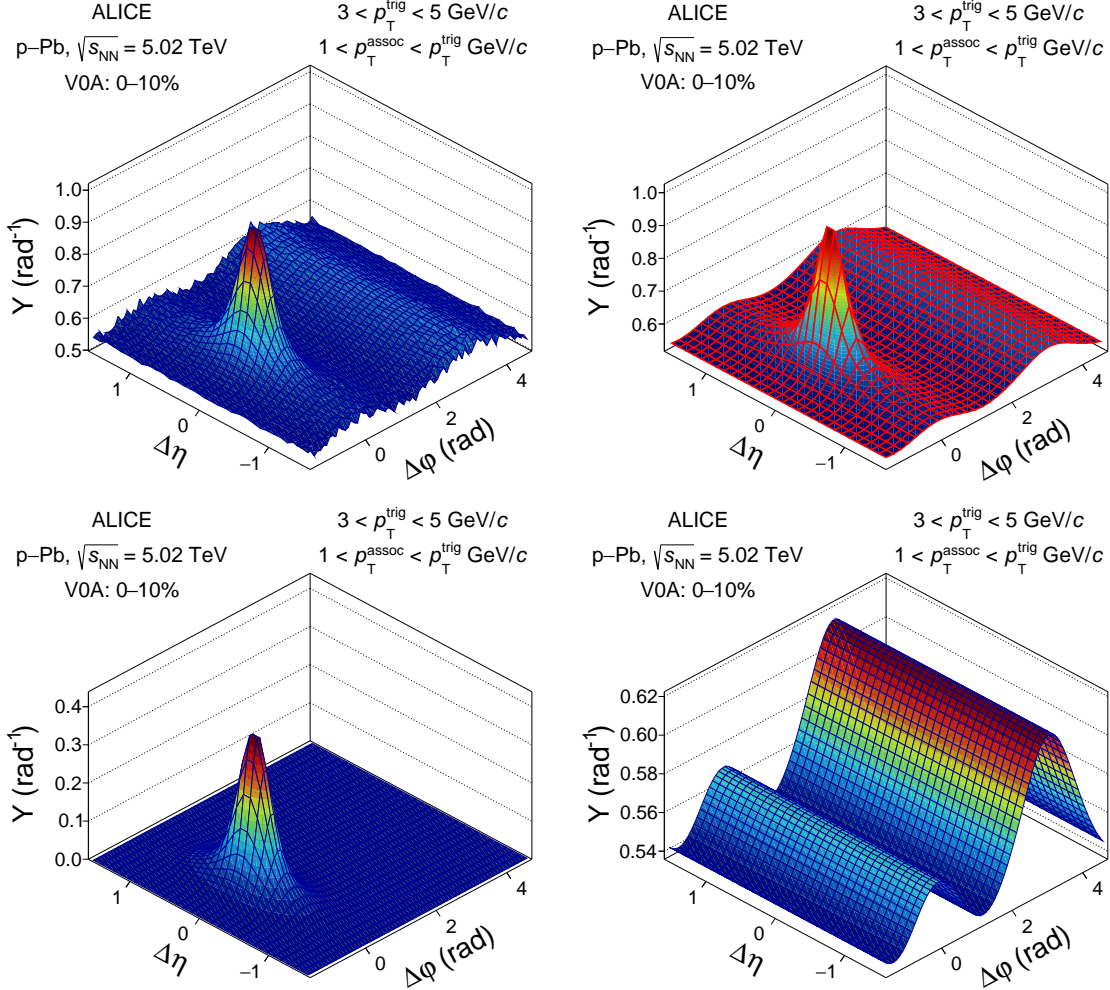


Figure 1: Top: raw associated yield per trigger particle Y (left) as a function of $\Delta\eta$ and $\Delta\varphi$ for pairs of charged particles measured in $|\eta| < 0.8$ with $3 < p_T^{\text{trig}} < 5 \text{ GeV}/c$ and $1 < p_T^{\text{assoc}} < p_T^{\text{trig}} \text{ GeV}/c$ in high-multiplicity (0–10%) p–Pb collisions at $\sqrt{s_{NN}} = 5.02$ TeV, and fit of the distribution (right). Bottom: extracted jet-particle (left) and background (right) yields.

3.1 Extraction of the near-side jet and background contributions

The two-dimensional correlation function is constructed as a function of the azimuthal angle difference ($\Delta\varphi$) and pseudorapidity difference ($\Delta\eta$) between trigger and associated particles (see Refs. [14, 49] and references therein). Only pairs of particles with the same electric charge are considered to suppress correlations originating from resonance decays. The p_T of trigger particles (p_T^{trig}) is taken to be larger than that of associated particles (p_T^{assoc}) to avoid double counting of pairs. The correlation distribution is corrected for the limited two-particle acceptance and detector inhomogeneities by using the event-mixing technique [50], and normalised to the total number of trigger particles. Therefore, the correlation function is expressed in terms of the associated yield per trigger particle Y as

$$Y = \frac{1}{N_{\text{trig}}} \frac{d^2 N_{\text{assoc}}}{d\Delta\eta d\Delta\varphi} = \frac{SE(\Delta\eta, \Delta\varphi)}{ME(\Delta\eta, \Delta\varphi)}, \quad (2)$$

where N_{trig} is the total number of trigger particles in a given event class. The signal distribution $SE(\Delta\eta, \Delta\varphi)$, given by $\frac{1}{N_{\text{trig}}} \frac{d^2 N_{\text{same}}}{d\Delta\eta d\Delta\varphi}$, corresponds to the associated yield per trigger particle for particle pairs from the

same event, and the background distribution $ME(\Delta\eta, \Delta\varphi) = \alpha \frac{d^2N_{\text{mix}}}{d\Delta\eta d\Delta\varphi}$ is obtained by correlating trigger particles in an event with associated particles from other events of same event class. The α factor is introduced to normalise the background distribution to unity in the region of maximum pair acceptance. The same strategy is employed in Pb–Pb collisions.

Figure 1 (top-left) shows a typical example of the two-dimensional correlation distribution in high-multiplicity (0–10%) p–Pb collisions at $\sqrt{s_{\text{NN}}} = 5.02$ TeV for $3 < p_{\text{T}}^{\text{trig}} < 5$ GeV/c and $1 < p_{\text{T}}^{\text{assoc}} < p_{\text{T}}^{\text{trig}}$ GeV/c. A near-side jet structure is clearly observed at $(\Delta\varphi \sim 0, \Delta\eta \sim 0)$ on top of the background. The distribution is fitted with a double Gaussian and a sum of Fourier harmonics up to the fifth order [51] (Fig. 1, top-right). The former is used to extract the near-side jet-peak yield (Fig. 1, bottom-left), and the latter serves to obtain the background yield (Fig. 1, bottom-right).

Similar typical distributions are also depicted in Fig. 2 for semicentral (20–60%) Pb–Pb collisions at $\sqrt{s_{\text{NN}}} = 5.02$ TeV for pairs of charged particles measured in $|\eta| < 0.8$ with $5 < p_{\text{T}}^{\text{trig}} < 6$ GeV/c and $2 < p_{\text{T}}^{\text{assoc}} < p_{\text{T}}^{\text{trig}}$ GeV/c in semicentral (20–60%) Pb–Pb collisions at $\sqrt{s_{\text{NN}}} = 5.02$ TeV. A near-side jet structure is also clearly observed at $(\Delta\varphi \sim 0, \Delta\eta \sim 0)$ on top of the background which is as expected, more important than in p–Pb collisions.

3.2 Determination of the v_2 coefficient of particle pairs

In the p–Pb analysis, the v_2 of particle pairs, $v_2(\Delta\varphi, \Delta\eta)$, is computed by using long-range three-particle correlations. The trigger particles in particle pairs for a given $(\Delta\varphi, \Delta\eta)$ cell are correlated with particles selected in $1.8 < \eta < 4.8$ using FMD1,2 to construct the long-range correlation distribution as a function of their azimuthal angle difference ($\Delta\varphi'$) and pseudorapidity difference ($\Delta\eta'$). Nonflow contributions, such as dijets, are suppressed by subtracting the scaled $(\Delta\varphi', \Delta\eta')$ correlation functions measured in low-multiplicity (60–100%) collisions following the procedure described in Refs. [19, 49, 52], where the scaling factor is the ratio of the away-side jet yield in high-multiplicity collisions to that in low-multiplicity collisions. For each $\Delta\varphi'$ interval, the $\Delta\eta'$ distribution in the $-5.6 < \Delta\eta' < -1.0$ range is integrated using a first-order polynomial fit to reduce the statistical fluctuations at the edges of $\Delta\eta'$ [52]. This $\Delta\varphi'$ distribution is fitted with a Fourier series parameterised with the first three harmonics as

$$\frac{dN}{d\Delta\varphi'} = a_0(\Delta\varphi, \Delta\eta) + 2 \sum_{n=1}^3 a_n(\Delta\varphi, \Delta\eta) \cos(n\Delta\varphi') \propto 1 + 2 \sum_{n=1}^3 V_{n\Delta}(\Delta\varphi, \Delta\eta) \cos(n\Delta\varphi'). \quad (3)$$

The $V_{2\Delta}(\Delta\varphi, \Delta\eta)$ second-order Fourier coefficient is extracted from the fit parameters and is further expressed relative to the baseline. The latter is estimated from the integral in $\Delta\varphi'$ of the scaled correlation distribution in the low-multiplicity class around the minimum. The procedure is repeated for each p_{T} interval of trigger and associated charged particles. Figure 3 shows an example of the per-trigger associated yield as a function of $\Delta\eta'$ and $\Delta\varphi'$ for $3 < p_{\text{T}}^{\text{trig}} < 5$ GeV/c, $1 < p_{\text{T}}^{\text{assoc}} < p_{\text{T}}^{\text{trig}}$ GeV/c, $-0.9 < \Delta\eta < -0.7$ and $3.7 < \Delta\varphi < 4.2$ in high-multiplicity (top-left) and low-multiplicity (top-right) p–Pb collisions. The per-trigger associated yield in high-multiplicity p–Pb collisions after the subtraction of the scaled correlation distribution in the low-multiplicity class and the fit of the corresponding distribution with Eq. (3) are displayed in the bottom-left and bottom-right panels, respectively.

Assuming that $V_{2\Delta}(\Delta\varphi, \Delta\eta)$ can be factorised as the product of single-particle v_2 coefficients, the v_2 of particle pairs represented by trigger particles ($v_2(\Delta\varphi, \Delta\eta)$) is expressed as the ratio between the $V_{2\Delta}(\Delta\varphi, \Delta\eta)$ and the v_2 of particles in FMD1,2 ($v_2^{\text{FMD1,2}}$). The $v_2^{\text{FMD1,2}}$ is obtained with the three-subevent technique [53] by constructing long-range two-particle correlations between trigger and associated particles in TPC–FMD1,2, TPC–FMD3 and FMD1,2–FMD3 [54]. If the factorisation holds, the $v_2^{\text{FMD1,2}}$

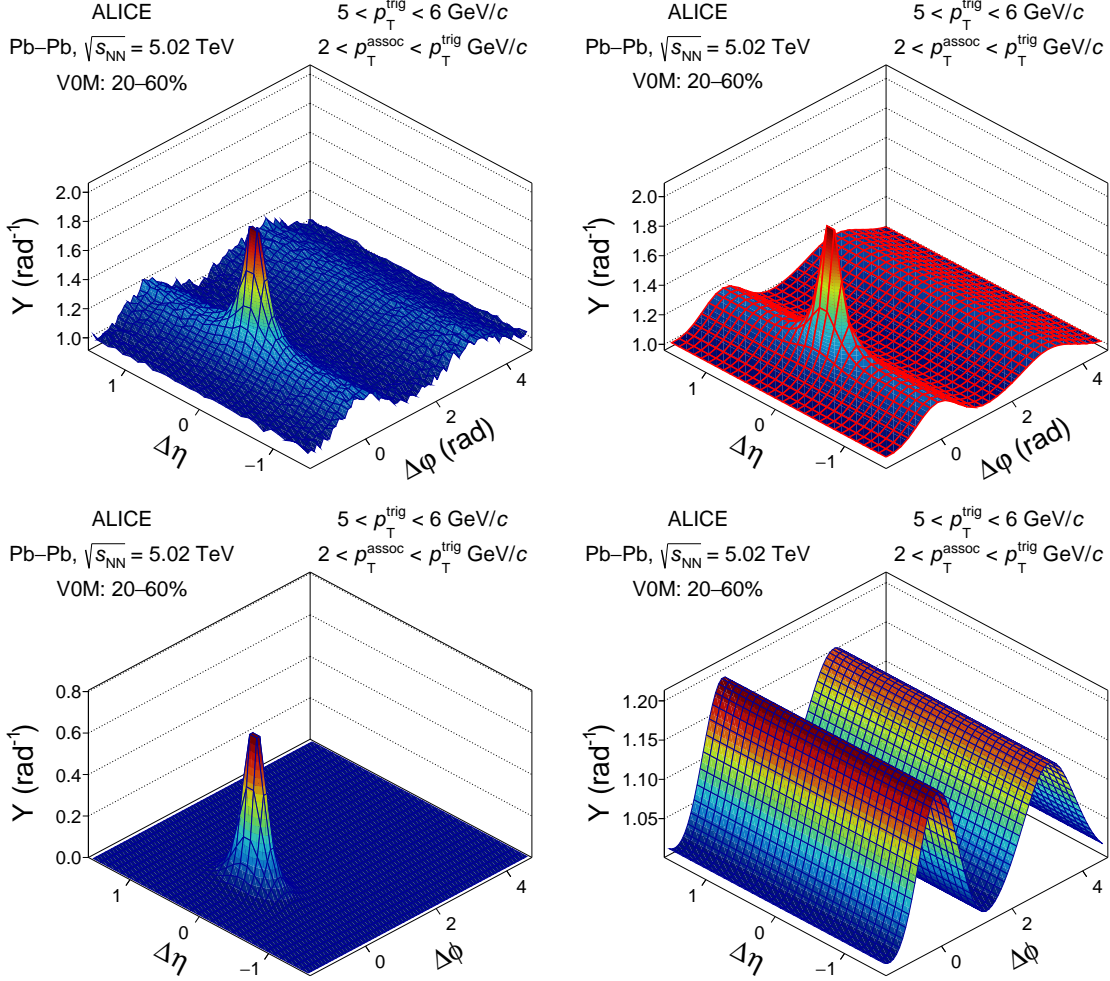


Figure 2: Top: raw associated yield per trigger particle Y (left) as a function of $\Delta\eta$ and $\Delta\varphi$ for pairs of charged particles measured in $|\eta| < 0.8$ with $5 < p_{\text{T}}^{\text{trig}} < 6 \text{ GeV}/c$ and $2 < p_{\text{T}}^{\text{assoc}} < p_{\text{T}}^{\text{trig}} \text{ GeV}/c$ in high-multiplicity (0–10%) Pb–Pb collisions at $\sqrt{s_{\text{NN}}} = 5.02 \text{ TeV}$, and fit of the distribution (right). Bottom: extracted jet-particle (left) and background (right) yields.

which is given by

$$v_2^{\text{FMD1,2}} = \sqrt{\frac{V_{2\Delta}^{\text{FMD1,2} - \text{FMD3}} V_{2\Delta}^{\text{TPC} - \text{FMD1,2}}}{V_{2\Delta}^{\text{TPC} - \text{FMD3}}}}, \quad (4)$$

amounts to 0.028 (with negligible uncertainties) in the 0–10% high-multiplicity class p–Pb collisions. The effect of the contamination of secondary particles is discussed in Section 3.3.

In Pb–Pb collisions, the $v_2(\Delta\varphi, \Delta\eta)$ coefficient is extracted from the scalar product method via the three-subevent technique [55, 56]. The method correlates particle pairs measured in the TPC with the second-order event flow vector $\mathbf{Q}_2^{\text{V0A}}$ estimated from the azimuthal distribution of the energy deposited in the V0A. Therefore, the resulting $v_2(\Delta\varphi, \Delta\eta)$ is defined as

$$v_2(\Delta\varphi, \Delta\eta) = \langle \mathbf{u}_2(\Delta\varphi, \Delta\eta) \cdot \mathbf{Q}_2^{\text{V0A}*} \rangle_{\text{TPC} - \text{TPC}} / \sqrt{\frac{\langle \mathbf{Q}_2^{\text{V0A}*} \cdot \mathbf{Q}_2^{\text{V0C}} \rangle \langle \mathbf{Q}_2^{\text{V0A}} \cdot \mathbf{Q}_2^{\text{SPD}*} \rangle}{\langle \mathbf{Q}_2^{\text{V0C}} \cdot \mathbf{Q}_2^{\text{SPD}*} \rangle}}, \quad (5)$$

where $\mathbf{u}_2(\Delta\varphi, \Delta\eta)$ is the unit flow vector of each particle measured in the TPC. The second-order harmonic event flow vectors $\mathbf{Q}_2^{\text{V0C}}$ and $\mathbf{Q}_2^{\text{SPD}}$ measured in the V0C and SPD, respectively, are introduced

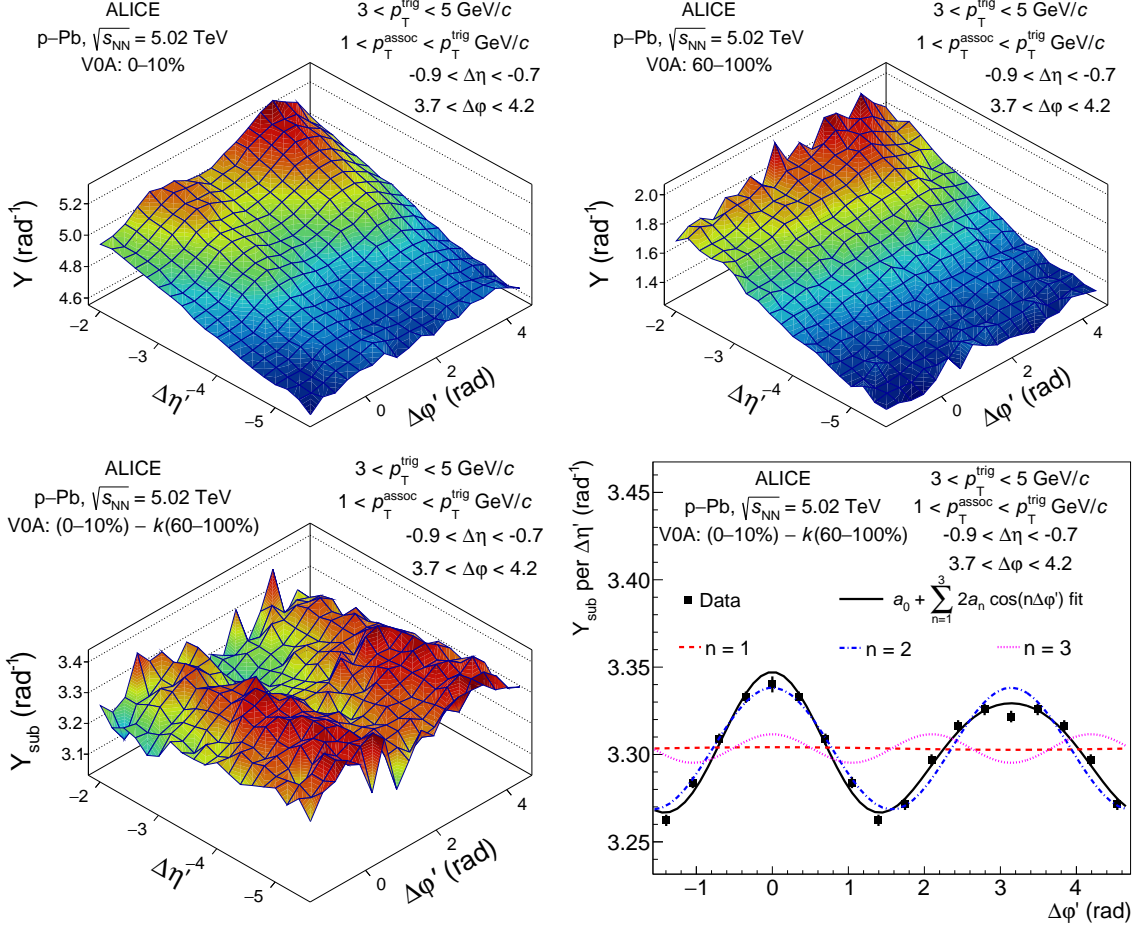


Figure 3: Top: example of the associated yield per-trigger particle Y in TPC–FMD1,2 correlations as a function of $\Delta\eta'$ and $\Delta\varphi'$ for $|\eta| < 0.8$ with $3 < p_T^{\text{trig}} < 5 \text{ GeV}/c$, $1 < p_T^{\text{assoc}} < p_T^{\text{trig}} \text{ GeV}/c$, $-0.9 < \Delta\eta < -0.7$ and $3.7 < \Delta\varphi < 4.2$ in high-multiplicity (left) and low-multiplicity (right) p–Pb collisions at $\sqrt{s_{\text{NN}}} = 5.02 \text{ TeV}$. Bottom: associated per-trigger yield after the subtraction of the scaled correlation distribution in low-multiplicity collisions(left)and fit of the distribution projected onto $\Delta\varphi'$ with Eq. (3).

to take into account the resolution of the event flow vector $\mathbf{Q}_2^{\text{V0A}}$. The symbol $*$ represents the complex conjugate and the bracket $\langle \dots \rangle_{\text{TPC–TPC}}$ denotes the average over charged-particle pairs in a given p_T interval for trigger and associated particles, and centrality range. The brackets in the denominator denote the average over all events in a centrality class containing the particle pair. A recentering procedure is applied to correct the event flow vectors for the non-uniform azimuthal acceptance effects of the corresponding detectors [57]. The pseudorapidity gaps between the TPC and V0A, and the V0A, V0C, and SPD detectors suppress nonflow effects [47] and eliminate autocorrelations [58].

In both p–Pb and Pb–Pb collisions, the $v_2(\Delta\varphi, \Delta\eta)$ can be written [58, 59] as the weighted sum of the v_2 of jet particles ($v_2^{\text{jet part}}$) and background ($v_2^B(\Delta\varphi)$), as

$$v_2(\Delta\varphi, \Delta\eta) = \frac{S(\Delta\varphi, \Delta\eta)}{S(\Delta\varphi, \Delta\eta) + B(\Delta\varphi, \Delta\eta)} v_2^{\text{jet part}} + \frac{B(\Delta\varphi, \Delta\eta)}{S(\Delta\varphi, \Delta\eta) + B(\Delta\varphi, \Delta\eta)} v_2^B(\Delta\varphi), \quad (6)$$

where the jet-particle $S(\Delta\varphi, \Delta\eta)$ and background $B(\Delta\varphi, \Delta\eta)$ yields are extracted from the two-particle correlation functions constructed in the TPC. The $v_2^{\text{jet part}}$ coefficient is obtained by parametrising $v_2^B(\Delta\varphi)$ with a Fourier series up to the fifth order and fitting Eq. (6) to the measured $v_2(\Delta\varphi, \Delta\eta)$ distributions in a given p_T interval for trigger and associated particles.

An example of the measured $v_2(\Delta\phi, \Delta\eta)$ distribution of particle pairs measured in p–Pb collisions at $\sqrt{s_{NN}} = 5.02$ TeV for $3 < p_T^{\text{trig}} < 5$ GeV/ c and $1 < p_T^{\text{assoc}} < p_T^{\text{trig}}$ GeV/ c is depicted in Fig. 4 (top-left), where a different structure is clearly seen in the region around the near-side jet peak ($\Delta\phi \sim 0, \Delta\eta \sim 0$) compared to the background-dominated region. This is a first indication of a different behaviour for v_2 of jet and background particles. A similar structure is also visible in Pb–Pb collisions at $\sqrt{s_{NN}} = 5.02$ TeV for $5 < p_T^{\text{trig}} < 6$ GeV/ c and $2 < p_T^{\text{assoc}} < p_T^{\text{trig}}$ GeV/ c (Fig. 4, bottom-left). The corresponding fits with Eq. (6) are shown in Fig. 4 (right panels).

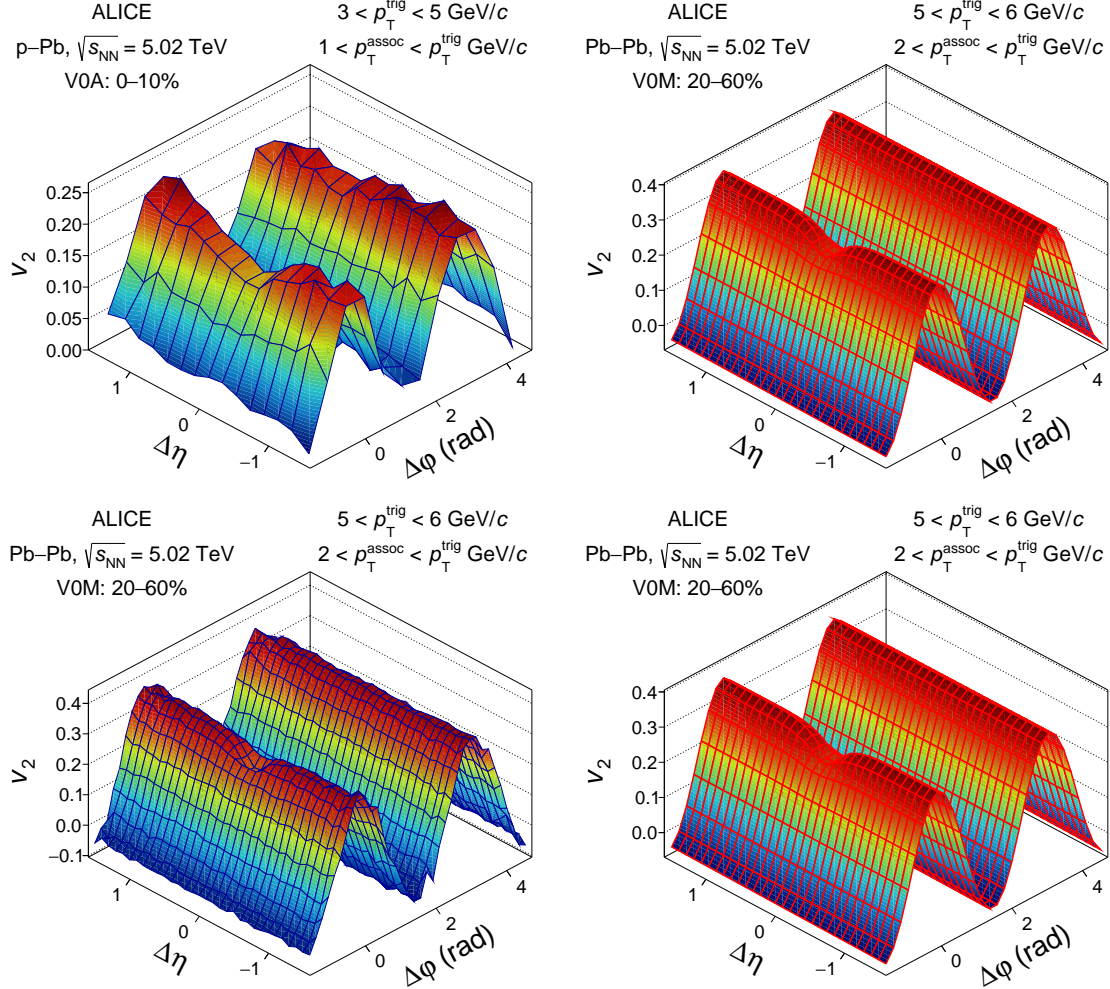


Figure 4: Left: $v_2(\Delta\phi, \Delta\eta)$ distributions of charged particles measured at midrapidity in high-multiplicity (0–10%) p–Pb collisions at $\sqrt{s_{NN}} = 5.02$ TeV (top) and semicentral (20–60%) Pb–Pb collisions at $\sqrt{s_{NN}} = 5.02$ TeV (bottom). Right: fits to the two corresponding distributions in p–Pb (top) and Pb–Pb (bottom) collisions. The p_T^{trig} and p_T^{assoc} intervals are mentioned in the legend.

For comparison, the v_2 coefficient of inclusive charged particles, v_2^{ch} is also computed. In p–Pb collisions, it is evaluated using the three-subevent technique by constructing long-range two-particle correlations, as done for the $v_2^{\text{FMD}1,2}$ calculation, and is expressed as

$$v_2^{\text{ch}} = \sqrt{\frac{V_{2\Delta}^{\text{TPC-FMD}1,2} V_{2\Delta}^{\text{TPC-FMD}3}}{V_{2\Delta}^{\text{FMD}1,2-\text{FMD}3}}}. \quad (7)$$

In Pb–Pb collisions, the v_2^{ch} is determined using the scalar product method with the three-subevent technique (see Eq. (5)).

3.3 Estimation of systematic uncertainties

Details of the separate contributions to the systematic uncertainties are given in Ref. [48]. The values for both jet particles in a representative p_T^{assoc} interval and inclusive charged particles in p–Pb and Pb–Pb collisions are summarised in Tables 1 and 2, respectively.

Table 1: Systematic uncertainties on the jet-particle v_2 for $p_T^{\text{assoc}} > 0.5 \text{ GeV}/c$ and the inclusive charged-particle v_2 in high-multiplicity (0–10%) p–Pb collisions at $\sqrt{s_{\text{NN}}} = 5.02 \text{ TeV}$. The systematic uncertainties vary within the indicated intervals depending on the p_T of trigger particles.

| Source | Jet particles $p_T^{\text{assoc}} > 0.5 \text{ GeV}/c$ | Charged particles |
|--------------------|-----------------------------------------------------------|-------------------|
| Vertex selection | 0.6–14.6% | 0.02–1.30% |
| FMD-V0 correlation | 0.1–7.9% | 0.1–0.2% |
| Track selection | 0.3–3.6% | 0.0–2.2% |
| Secondaries in FMD | 4% | 4% |
| Residual nonflow | 0.1–5.4% | 0.1–13.2% |
| Remaining ridge | 6.5–29.0% | 0.7–20.7% |
| v_2 calculation | 4.5–11.7% | 0.7–1.5% |
| Total | 11.2–34.3% | 4.4–25.3% |

The jet-particle and inclusive charged-particle v_2 measurements in p–Pb collisions are affected by the following systematic uncertainties. The variation of the range of z_{vtx} and a less stringent condition on the correlation between the multiplicity estimates obtained with the FMD and V0, give the systematic uncertainties related to the event selection. The uncertainty on the track reconstruction is estimated by modifying the track selection criteria. The bias due to the contribution of secondary particles produced in the FMD acceptance on the jet-particle v_2 is investigated in AMPT simulations [36, 37, 60]. In order to check for residual nonflow effects after the subtraction of the scaled low-multiplicity event class, the template fitting procedure [19] is tested. The difference between the two procedures is considered as a systematic uncertainty. A potential bias resulting from weak long-range correlations present in 60–100% low-multiplicity events is studied by changing the interval from 60–100% to 70–100%. A systematic effect arises from the procedure employed for the $\Delta\varphi'$. The $\Delta\varphi'$ projection in Eq. (3) is obtained from a constant fit instead of using a first-order polynomial fit along each $\Delta\eta'$ interval. Finally, the baseline is also calculated in high-multiplicity collisions from the integral or from a second-order polynomial fit around the minimum at $\Delta\varphi' \sim \pi/2$. The last two sources are the systematic uncertainty on the v_2 calculation. The aforementioned sources are added in quadrature in each p_T interval of trigger and associated particles to obtain a total systematic uncertainty on the jet-particle v_2 in the range 11.2–34.3%. The total systematic uncertainty on the inclusive charged-particle which depends on the trigger-particle p_T , is 4.4–25.3%.

In Pb–Pb collisions, in addition to the systematic uncertainties arising from the variation of the z_{vtx} range and track selection criteria listed for p–Pb collisions, a systematic uncertainty related to the centrality determination is estimated by using different centrality estimators. The systematic effect related to the pile-up event rejection is assessed via a dedicated analysis where pile-up events are not removed, only to estimate their importance. The event flow vector is computed by using V0C instead of V0A. All the systematic uncertainties are added in quadrature to obtain the total systematic uncertainty ranging from 1.6–10.1% and 0.02–7.30% for the jet-particle v_2 and inclusive charged-particle v_2 , respectively.

Table 2: Systematic uncertainties on the jet-particle v_2 for $p_T^{\text{assoc}} > 2.0 \text{ GeV}/c$ and the inclusive charged-particle v_2 in semicentral (20–60%) Pb–Pb collisions at $\sqrt{s_{\text{NN}}} = 5.02 \text{ TeV}$. The systematic uncertainties vary within the indicated intervals depending on the p_T of trigger particles.

| Source | Jet particles $p_T^{\text{assoc}} > 2 \text{ GeV}/c$ | Charged particles |
|------------------|---------------------------------------------------------|-------------------|
| Vertex selection | 0.6–5.3% | 0–5.3% |
| Pile-up | 0.01–3.60% | 0–2.7% |
| Centrality | 0.3–1.4% | 0–1.8% |
| Flow vector | 0.3–1.4% | 0–4.2% |
| Track selection | 0.8–4.5% | 0.01–1.80% |
| Total | 1.6–7.3% | 0.02–7.30% |

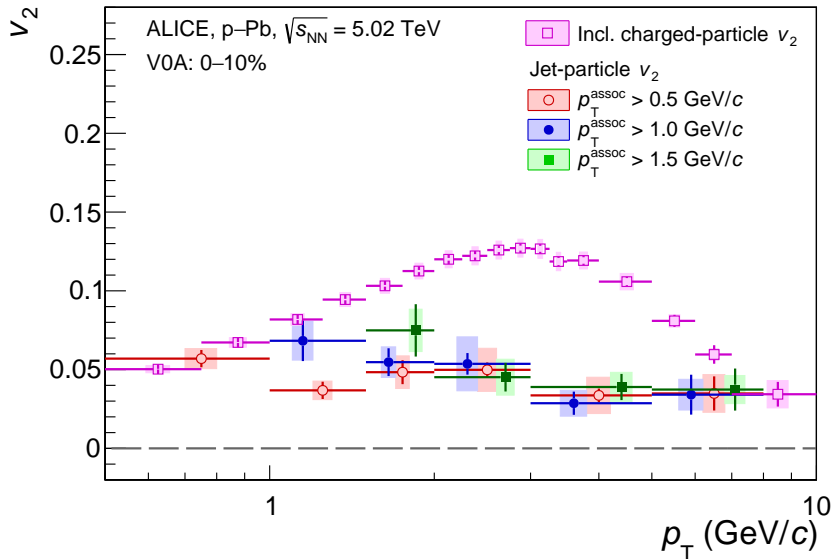


Figure 5: Jet-particle v_2 as a function of the trigger-particle p_T for several p_T^{assoc} intervals in 0–10% p–Pb collisions at $\sqrt{s_{\text{NN}}} = 5.02 \text{ TeV}$, compared with the inclusive charged-particle v_2 . The values of the jet-particle v_2 are horizontally shifted around the centre of the bin for better visibility. The statistical uncertainties, shown as vertical bars, are determined using the sub-sample technique. The systematic uncertainties are represented as filled boxes. Horizontal bars indicate the bin width.

4 Results and model comparisons

Figure 5 presents the v_2 of jet particles as a function of p_T at midrapidity ($|\eta| < 0.8$) for different p_T^{assoc} intervals, in high-multiplicity (0–10%) p–Pb collisions at $\sqrt{s_{\text{NN}}} = 5.02 \text{ TeV}$. The p_T -differential inclusive charged-particle v_2 coefficient is also displayed. A positive jet-particle v_2 of ~ 0.04 is measured and it is independent of the p_T of trigger and associated particles within uncertainties. The significance is $2.6\text{--}6.8\sigma$ for $p_T \lesssim 5 \text{ GeV}/c$, depending on both the p_T of trigger and associated particles. In contrast, the v_2 of inclusive charged particles which mostly originates from the underlying event, is larger in magnitude and presents a clear dependence on p_T . This constitutes the first experimental evidence of different mechanisms in play for the v_2 of soft and hard probes at low p_T in p–Pb collisions.

The jet-particle v_2 and the inclusive charged-particle v_2 are also measured in semicentral (20–60%) Pb–Pb collisions at $\sqrt{s_{\text{NN}}} = 5.02 \text{ TeV}$, as shown in Fig. 6. The published v_2 of reconstructed jets measured in 30–50% Pb–Pb collisions at $\sqrt{s_{\text{NN}}} = 2.76 \text{ TeV}$ [35] is also displayed, extending the presented measurements up to $p_T = 90 \text{ GeV}/c$. A positive jet-particle v_2 is measured for the first time in the low

p_T region, down to $p_T = 2 \text{ GeV}/c$. The jet-particle v_2 does not exhibit any dependence on the associated p_T , while it decreases with increasing p_T from $p_T \sim 3 \text{ GeV}/c$, and converges towards the v_2 of inclusive charged particles for $p_T \gtrsim 7 \text{ GeV}/c$. In the high p_T region ($p_T \gtrsim 10 \text{ GeV}/c$), the uniform behaviour of the inclusive charged-particle v_2 and jet v_2 as a function of p_T is attributed to the path-length dependent parton energy loss in Pb–Pb collisions [46]. It can be noted that in this region, the jet-particle v_2 is consistent with the reconstructed jet v_2 . In the interval $2 < p_T \lesssim 6 \text{ GeV}/c$, the clear p_T dependence of the jet-particle v_2 in Pb–Pb collisions may be attributed to the interplay between hard partons and bulk particles.

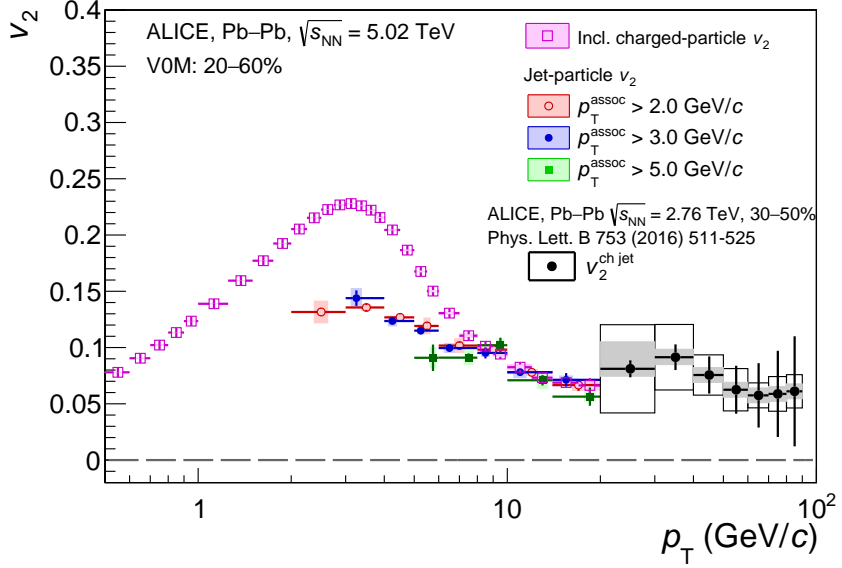


Figure 6: Jet-particle v_2 as a function of the trigger-particle p_T for several p_T^{assoc} intervals in 20–60% Pb–Pb collisions at $\sqrt{s_{\text{NN}}} = 5.02 \text{ TeV}$, compared with the inclusive charged-particle v_2 . The values of the jet-particle v_2 are horizontally shifted around the centre of the bin for better visibility. The statistical uncertainties, shown as vertical bars, are determined using the sub-sample technique. The systematic uncertainties are represented as filled boxes. Horizontal bars indicate the bin width. The published v_2 of reconstructed jets measured in 30–50% Pb–Pb collisions is also shown [35].

The comparison of the v_2 results obtained in p–Pb (0–10%) and Pb–Pb (20–60%) collisions for jet particles and inclusive charged particles is discussed in Fig. 7. Since no significant dependence on p_T^{assoc} is evidenced for jet particles (see Figs. 5 and 6), the results are shown for the p_T^{assoc} interval which allows us to cover the largest p_T range. The centrality class is chosen such that the eccentricity, which quantifies the initial spatial anisotropies, is close to that in high-multiplicity p–Pb collisions according to Glauber Monte Carlo simulations [61], although the charged-particle multiplicities reached in the heavier system are larger. The published v_2 of reconstructed jets measured in 30–50% Pb–Pb collisions at $\sqrt{s_{\text{NN}}} = 2.76 \text{ TeV}$ [35] are also included in the figure. A scaling factor of 0.6 is applied to the v_2 of inclusive charged particles, jet particles and reconstructed jets in Pb–Pb collisions to ensure that the low p_T ($p_T \lesssim 3 \text{ GeV}/c$) inclusive charged-particle v_2 matches that in p–Pb collisions. This factor may account for the slightly different spatial anisotropies in the two colliding systems and the larger multiplicity in the heaviest system [17]. After such scaling, the inclusive charged-particle v_2 in p–Pb collisions is compatible with that measured in Pb–Pb collisions. A different behaviour is evidenced for jet particles. In contrast to what is observed in Pb–Pb collisions, the jet-particle v_2 measured in p–Pb collisions is found independent of p_T . This suggests that the collectivity from the initial state survives throughout all stages in the system evolution more easily in p–Pb than Pb–Pb collisions [62]. This is also confirmed from the positive jet-particle v_2 measurement in p–Pb collisions without any indication of a modification of the jet production

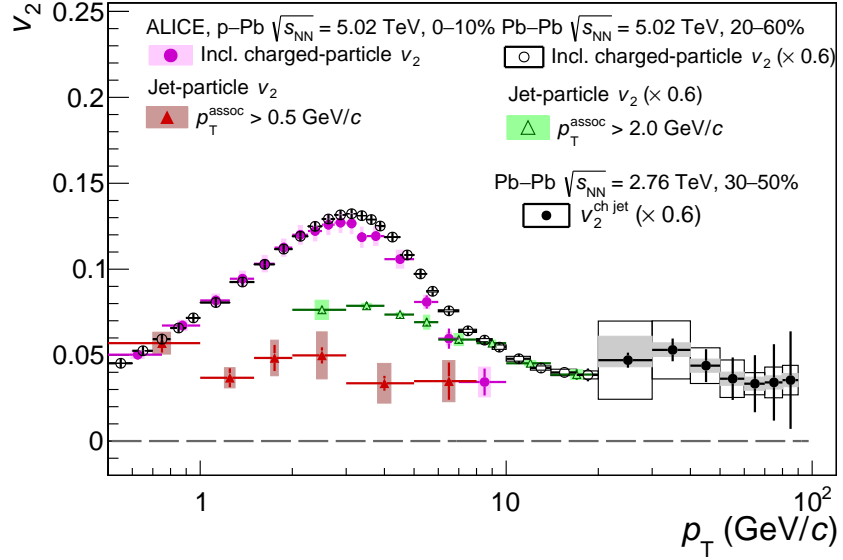


Figure 7: Comparison of the p_T -differential jet-particle and inclusive charged-particle v_2 measured in high-multiplicity p–Pb collisions at $\sqrt{s_{NN}} = 5.02$ TeV, 0–10% Pb–Pb $\sqrt{s_{NN}} = 5.02$ TeV, 20–60%. The published ALICE v_2 of reconstructed jets measured in 30–50% Pb–Pb collisions is also shown [35]. The results obtained in Pb–Pb collisions are scaled by a factor 0.6. See the text for the details.

yields within experimental uncertainties [17, 25, 26].

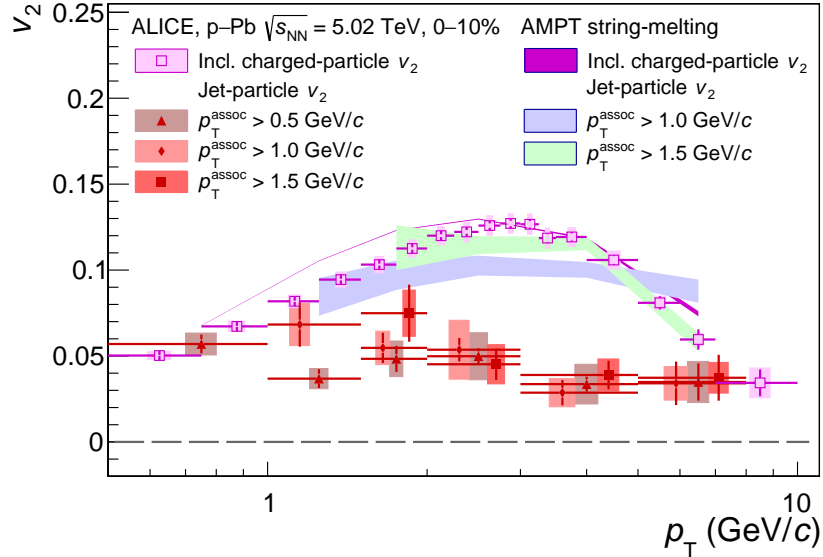


Figure 8: Comparison of the p_T -differential jet-particle and inclusive charged-particle v_2 measured in high-multiplicity p–Pb collisions at $\sqrt{s_{NN}} = 5.02$ TeV with AMPT calculations [36, 37].

Figure 8 presents a comparison of the jet-particle and inclusive charged-particle v_2 with the string-melting version of AMPT model (v2.26t9b) [36, 37, 60] in order to shed more light on the origin of the jet-particle v_2 measured in high-multiplicity p–Pb collisions. The AMPT model includes four main processes: i) initial conditions obtained from the HIJING model [63, 64], ii) parton scatterings based on the Zhang’s parton cascade (ZPC) model [65], iii) hadronisation via coalescence and (iv) hadronic interactions described by a relativistic transport (ART) model [66]. A parton scattering cross section of 3

mb is used [67]. Its value is obtained by adjusting the Debye screening mass so that the model describes the p_T distribution and the v_2 coefficient of identified particles measured in p–Pb collisions at $\sqrt{s_{NN}} = 5.02$ TeV by the ALICE Collaboration [68]. In this model, the v_2 is calculated following the same analysis procedure as with data and the event characterisation is done by mimicking the event class selection using the V0A detector at particle level, i.e. by counting charged particles in $2.8 < \eta < 5.1$. The AMPT calculations lead to a positive inclusive charged-particle and jet-particle v_2 , indicating that parton interactions play an important role in the v_2 generation. The model provides a fair agreement with the measured inclusive charged-particle v_2 , while it overestimates the measured jet-particle v_2 , predicting a v_2 whose shape and magnitude are compatible with those of inclusive charged particles. This is possibly due to the fact that AMPT treats soft and hard components equally in the parton interaction stage, while the measurement indicates that hard partons interact with the underlying event differently from the bulk constituents themselves.

5 Summary

In summary, the jet-particle v_2 measured in high-multiplicity (0–10%) p–Pb collisions at $\sqrt{s_{NN}} = 5.02$ TeV is assessed for the first time in the p_T range 0.5–8.0 GeV/ c by means of a novel multi-particle correlation technique. The jet-particle v_2 is also measured down to low p_T in semicentral Pb–Pb collisions at $\sqrt{s_{NN}} = 5.02$ TeV and is complementary to the previous jet v_2 results at higher p_T . Comparisons with the inclusive charged-particle v_2 measured in both p–Pb and Pb–Pb collisions are discussed. A positive and p_T -independent v_2 signal is observed with a significance reaching 6.8σ at low p_T in p–Pb collisions. The v_2 magnitude is smaller than that measured in Pb–Pb collisions at intermediate p_T . In addition, a clear p_T dependence of the v_2 signal of jet particles is observed in Pb–Pb collisions. The comparison with AMPT predictions shows that parton interactions can generate a positive v_2 for jet particles in high-multiplicity p–Pb collisions. These new results bring crucial information about the origin of the observed azimuthal anisotropies of jet particles in p–Pb collisions and set key constraints on theoretical calculations.

Acknowledgements

The ALICE Collaboration would like to thank all its engineers and technicians for their invaluable contributions to the construction of the experiment and the CERN accelerator teams for the outstanding performance of the LHC complex. The ALICE Collaboration gratefully acknowledges the resources and support provided by all Grid centres and the Worldwide LHC Computing Grid (WLCG) collaboration. The ALICE Collaboration acknowledges the following funding agencies for their support in building and running the ALICE detector: A. I. Alikhanyan National Science Laboratory (Yerevan Physics Institute) Foundation (ANSL), State Committee of Science and World Federation of Scientists (WFS), Armenia; Austrian Academy of Sciences, Austrian Science Fund (FWF): [M 2467-N36] and Nationalstiftung für Forschung, Technologie und Entwicklung, Austria; Ministry of Communications and High Technologies, National Nuclear Research Center, Azerbaijan; Conselho Nacional de Desenvolvimento Científico e Tecnológico (CNPq), Financiadora de Estudos e Projetos (Finep), Fundação de Amparo à Pesquisa do Estado de São Paulo (FAPESP) and Universidade Federal do Rio Grande do Sul (UFRGS), Brazil; Bulgarian Ministry of Education and Science, within the National Roadmap for Research Infrastructures 2020-2027 (object CERN), Bulgaria; Ministry of Education of China (MOEC) , Ministry of Science & Technology of China (MSTC) and National Natural Science Foundation of China (NSFC), China; Ministry of Science and Education and Croatian Science Foundation, Croatia; Centro de Aplicaciones Tecnológicas y Desarrollo Nuclear (CEADEN), Cubaenergía, Cuba; Ministry of Education, Youth and Sports of the Czech Republic, Czech Republic; The Danish Council for Independent Research | Natural Sciences, the VILLUM FONDEN and Danish National Research Foundation (DNRF), Denmark; Helsinki Institute of Physics (HIP), Finland; Commissariat à l’Energie Atomique (CEA) and Institut National de Physique Nucléaire et de Physique des Particules (IN2P3) and Centre National de la

Recherche Scientifique (CNRS), France; Bundesministerium für Bildung und Forschung (BMBF) and GSI Helmholtzzentrum für Schwerionenforschung GmbH, Germany; General Secretariat for Research and Technology, Ministry of Education, Research and Religions, Greece; National Research, Development and Innovation Office, Hungary; Department of Atomic Energy Government of India (DAE), Department of Science and Technology, Government of India (DST), University Grants Commission, Government of India (UGC) and Council of Scientific and Industrial Research (CSIR), India; National Research and Innovation Agency - BRIN, Indonesia; Istituto Nazionale di Fisica Nucleare (INFN), Italy; Japanese Ministry of Education, Culture, Sports, Science and Technology (MEXT) and Japan Society for the Promotion of Science (JSPS) KAKENHI, Japan; Consejo Nacional de Ciencia (CONACYT) y Tecnología, through Fondo de Cooperación Internacional en Ciencia y Tecnología (FONCICYT) and Dirección General de Asuntos del Personal Académico (DGAPA), Mexico; Nederlandse Organisatie voor Wetenschappelijk Onderzoek (NWO), Netherlands; The Research Council of Norway, Norway; Commission on Science and Technology for Sustainable Development in the South (COMSATS), Pakistan; Pontificia Universidad Católica del Perú, Peru; Ministry of Education and Science, National Science Centre and WUT ID-UB, Poland; Korea Institute of Science and Technology Information and National Research Foundation of Korea (NRF), Republic of Korea; Ministry of Education and Scientific Research, Institute of Atomic Physics, Ministry of Research and Innovation and Institute of Atomic Physics and Universitatea Națională de Știință și Tehnologie Politehnica București, Romania; Ministry of Education, Science, Research and Sport of the Slovak Republic, Slovakia; National Research Foundation of South Africa, South Africa; Swedish Research Council (VR) and Knut & Alice Wallenberg Foundation (KAW), Sweden; European Organization for Nuclear Research, Switzerland; Suranaree University of Technology (SUT), National Science and Technology Development Agency (NSTDA) and National Science, Research and Innovation Fund (NSRF via PMU-B B05F650021), Thailand; Turkish Energy, Nuclear and Mineral Research Agency (TENMAK), Turkey; National Academy of Sciences of Ukraine, Ukraine; Science and Technology Facilities Council (STFC), United Kingdom; National Science Foundation of the United States of America (NSF) and United States Department of Energy, Office of Nuclear Physics (DOE NP), United States of America. In addition, individual groups or members have received support from: European Research Council, Strong 2020 - Horizon 2020, Marie Skłodowska Curie (grant nos. 950692, 824093, 896850), European Union; ICSC - Centro Nazionale di Ricerca in High Performance Computing, Big Data and Quantum Computing, European Union - NextGenerationEU; Academy of Finland (Center of Excellence in Quark Matter) (grant nos. 346327, 346328), Finland; Programa de Apoyos para la Superación del Personal Académico, UNAM, Mexico.

References

- [1] **HotQCD** Collaboration, A. Bazavov *et al.*, “Equation of state in (2+1)-flavor QCD”, *Phys. Rev. D* **90** (2014) 094503, arXiv:1407.6387 [hep-lat].
- [2] E. Shuryak, “Strongly coupled quark-gluon plasma in heavy ion collisions”, *Rev. Mod. Phys.* **89** (2017) 035001, arXiv:1412.8393 [hep-ph].
- [3] S. Voloshin and Y. Zhang, “Flow study in relativistic nuclear collisions by Fourier expansion of Azimuthal particle distributions”, *Z. Phys. C* **70** (1996) 665–672, arXiv:hep-ph/9407282.
- [4] A. M. Poskanzer and S. Voloshin, “Methods for analyzing anisotropic flow in relativistic nuclear collisions”, *Phys. Rev. C* **58** (1998) 1671–1678, arXiv:nucl-ex/9805001.
- [5] J.-Y. Ollitrault, “Anisotropy as a signature of transverse collective flow”, *Phys. Rev. D* **46** (1992) 229–245.
- [6] P. F. Kolb and U. W. Heinz, “Hydrodynamic description of ultrarelativistic heavy ion collisions”, *SUNY-NTG-03-06* (2003) 634–714, arXiv:nucl-th/0305084.

- [7] M. Gyulassy, I. Vitev, and X. Wang, “High p_T azimuthal asymmetry in noncentral A+A at RHIC”, *Phys. Rev. Lett.* **86** (2001) 2537–2540, arXiv:nucl-th/0012092.
- [8] E. Shuryak, “Azimuthal asymmetry at large p_T seem to be too large for a pure ‘jet quenching’”, *Phys. Rev. C* **66** (2002) 027902, arXiv:nucl-th/0112042.
- [9] K. J. Eskola, H. Paukkunen, and C. A. Salgado, “EPS09: A New Generation of NLO and LO Nuclear Parton Distribution Functions”, *JHEP* **04** (2009) 065, arXiv:0902.4154 [hep-ph].
- [10] B. Z. Kopeliovich, J. Nemchik, A. Schafer, and A. V. Tarasov, “Cronin effect in hadron production off nuclei”, *Phys. Rev. Lett.* **88** (2002) 232303, arXiv:hep-ph/0201010 [hep-ph].
- [11] Z.-B. Kang, I. Vitev, E. Wang, H. Xing, and C. Zhang, “Multiple scattering effects on heavy meson production in p+A collisions at backward rapidity”, *Phys. Lett. B* **740** (2015) 23–29, arXiv:1409.2494 [hep-ph].
- [12] **ALICE** Collaboration, S. Acharya *et al.*, “Azimuthal Anisotropy of Heavy-Flavor Decay Electrons in p–Pb Collisions at $\sqrt{s_{\text{NN}}} = 5.02 \text{ TeV}$ ”, *Phys. Rev. Lett.* **122** (2019) 072301, arXiv:1805.04367 [nucl-ex].
- [13] **CMS** Collaboration, A. M. Sirunyan *et al.*, “Studies of charm and beauty hadron long-range correlations in pp and pPb collisions at LHC energies”, *Phys. Lett. B* **813** (2021) 136036, arXiv:2009.07065 [hep-ex].
- [14] **ALICE** Collaboration, S. Acharya *et al.*, “Search for collectivity with azimuthal J/ψ -hadron correlations in high multiplicity p–Pb collisions at $\sqrt{s_{\text{NN}}} = 5.02$ and 8.16 TeV ”, *Phys. Lett. B* **780** (2018) 7–20, arXiv:1709.06807 [nucl-ex].
- [15] **CMS** Collaboration, A. M. Sirunyan *et al.*, “Observation of prompt J/ψ meson elliptic flow in high-multiplicity pPb collisions at $\sqrt{s_{\text{NN}}} = 8.16 \text{ TeV}$ ”, *Phys. Lett. B* **791** (2019) 172–194, arXiv:1810.01473 [hep-ex].
- [16] **CMS** Collaboration, A. M. Sirunyan *et al.*, “Pseudorapidity and transverse momentum dependence of flow harmonics in pPb and PbPb collisions”, *Phys. Rev. C* **98** (2018) 044902, arXiv:1710.07864 [nucl-ex].
- [17] **ATLAS** Collaboration, G. Aad *et al.*, “Transverse momentum and process dependent azimuthal anisotropies in $\sqrt{s_{\text{NN}}} = 8.16 \text{ TeV}$ p+Pb collisions with the ATLAS detector”, *Eur. Phys. J. C* **80** (2020) 73, arXiv:1910.13978 [nucl-ex].
- [18] **ATLAS** Collaboration, G. Aad *et al.*, “Observation of Long-Range Elliptic Azimuthal Anisotropies in $\sqrt{s} = 13$ and 2.76 TeV pp Collisions with the ATLAS Detector”, *Phys. Rev. Lett.* **116** (2016) 172301, arXiv:1509.04776 [hep-ex].
- [19] **ATLAS** Collaboration, M. Aaboud *et al.*, “Measurements of long-range azimuthal anisotropies and associated Fourier coefficients for pp collisions at $\sqrt{s} = 5.02$ and 13 TeV and p+Pb collisions at $\sqrt{s_{\text{NN}}} = 5.02 \text{ TeV}$ with the ATLAS detector”, *Phys. Rev. C* **96** (2017) 024908, arXiv:1609.06213 [nucl-ex].
- [20] **ATLAS** Collaboration, M. Aaboud *et al.*, “Measurement of multi-particle azimuthal correlations in pp, p+Pb and low-multiplicity Pb+Pb collisions with the ATLAS detector”, *Eur. Phys. J. C* **77** (2017) 428, arXiv:1705.04176 [hep-ex].
- [21] **CMS** Collaboration, A. M. Sirunyan *et al.*, “Observation of Correlated Azimuthal Anisotropy Fourier Harmonics in pp and p + Pb Collisions at the LHC”, *Phys. Rev. Lett.* **120** (2018) 092301, arXiv:1709.09189 [nucl-ex].

- [22] ALICE Collaboration, S. Acharya *et al.*, “Investigations of Anisotropic Flow Using Multiparticle Azimuthal Correlations in pp, p–Pb, Xe–Xe, and Pb–Pb Collisions at the LHC”, *Phys. Rev. Lett.* **123** (2019) 142301, arXiv:1903.01790 [nucl-ex].
- [23] ATLAS Collaboration, G. Aad *et al.*, “Measurement of azimuthal anisotropy of muons from charm and bottom hadrons in pp collisions at $\sqrt{s} = 13$ TeV with the ATLAS detector”, *Phys. Rev. Lett.* **124** (2020) 082301, arXiv:1909.01650 [nucl-ex].
- [24] ALICE Collaboration, J. Adam *et al.*, “Centrality dependence of particle production in p–Pb collisions at $\sqrt{s_{\text{NN}}} = 5.02$ TeV”, *Phys. Rev. C* **91** (2015) 064905, arXiv:1412.6828 [nucl-ex].
- [25] ALICE Collaboration, J. Adam *et al.*, “Measurement of charged jet production cross sections and nuclear modification in p–Pb collisions at $\sqrt{s_{\text{NN}}} = 5.02$ TeV”, *Phys. Lett. B* **749** (2015) 68–81, arXiv:1503.00681 [nucl-ex].
- [26] ALICE Collaboration, J. Adam *et al.*, “Centrality dependence of charged jet production in p–Pb collisions at $\sqrt{s_{\text{NN}}} = 5.02$ TeV”, *Eur. Phys. J. C* **76** (2016) 271, arXiv:1603.03402 [nucl-ex].
- [27] ATLAS Collaboration, G. Aad *et al.*, “Transverse momentum, rapidity, and centrality dependence of inclusive charged-particle production in $\sqrt{s_{\text{NN}}} = 5.02$ TeV $p + \text{Pb}$ collisions measured by the ATLAS experiment”, *Phys. Lett. B* **763** (2016) 313–336, arXiv:1605.06436 [hep-ex].
- [28] ALICE Collaboration, S. Acharya *et al.*, “Measurement of electrons from heavy-flavour hadron decays as a function of multiplicity in p–Pb collisions at $\sqrt{s_{\text{NN}}} = 5.02$ TeV”, *JHEP* **02** (2020) 077, arXiv:1910.14399 [nucl-ex].
- [29] ALICE Collaboration, S. Acharya *et al.*, “Measurement of prompt D^0 , D^+ , D^{*+} , and D_S^+ production in p–Pb collisions at $\sqrt{s_{\text{NN}}} = 5.02$ TeV”, *JHEP* **12** (2019) 092, arXiv:1906.03425 [nucl-ex].
- [30] K. Dusling and R. Venugopalan, “Evidence for BFKL and saturation dynamics from dihadron spectra at the LHC”, *Phys. Rev. D* **87** (2013) 051502, arXiv:1210.3890 [hep-ph].
- [31] K. Dusling and R. Venugopalan, “Comparison of the color glass condensate to dihadron correlations in proton-proton and proton-nucleus collisions”, *Phys. Rev. D* **87** (2013) 094034, arXiv:1302.7018 [hep-ph].
- [32] K. Dusling, W. Li, and B. Schenke, “Novel collective phenomena in high-energy proton–proton and proton–nucleus collisions”, *Int. J. Mod. Phys. E* **25** (2016) 1630002, arXiv:1509.07939 [nucl-ex].
- [33] C. Zhang, C. Marquet, G.-Y. Qin, Y. Shi, L. Wang, S.-Y. Wei, and B.-W. Xiao, “Collectivity of heavy mesons in proton-nucleus collisions”, *Phys. Rev. D* **102** (2020) 034010, arXiv:2002.09878 [hep-ph].
- [34] L. He, T. Edmonds, Z.-W. Lin, F. Liu, D. Molnar, and F. Wang, “Anisotropic parton escape is the dominant source of azimuthal anisotropy in transport models”, *Phys. Lett. B* **753** (2016) 506–510, arXiv:1502.05572 [nucl-th].
- [35] ALICE Collaboration, J. Adam *et al.*, “Azimuthal anisotropy of charged jet production in $\sqrt{s_{\text{NN}}} = 2.76$ TeV Pb–Pb collisions”, *Phys. Lett. B* **753** (2016) 511–525, arXiv:1509.07334 [nucl-ex].
- [36] Z.-W. Lin, C. M. Ko, B.-A. Li, B. Zhang, and S. Pal, “A Multi-Phase Transport Model for Relativistic Heavy Ion Collisions”, *Phys. Rev. C* **72** (2005) 064901, arXiv:nucl-th/0411110.

- [37] H. Li, Z.-W. Lin, and F. Wang, “Charm quarks are more hydrodynamic than light quarks in final-state elliptic flow”, *Phys. Rev. C* **99** (2019) 044911, arXiv:1804.02681 [hep-ph].
- [38] ALICE Collaboration, K. Aamodt *et al.*, “The ALICE experiment at the CERN LHC”, *JINST* **3** (2008) S08002.
- [39] ALICE Collaboration, B. Abelev *et al.*, “Performance of the ALICE Experiment at the CERN LHC”, *Int. J. Mod. Phys. A* **29** (2014) 1430044, arXiv:1402.4476 [nucl-ex].
- [40] J. Alme *et al.*, “The ALICE TPC, a large 3-dimensional tracking device with fast readout for ultra-high multiplicity events”, *Nucl. Instrum. Meth. A* **622** (2010) 316–367, arXiv:1001.1950 [physics.ins-det].
- [41] ALICE Collaboration, K. Aamodt *et al.*, “Alignment of the ALICE Inner Tracking System with cosmic-ray tracks”, *JINST* **5** (2010) P03003, arXiv:1001.0502 [physics.ins-det].
- [42] ALICE Collaboration, *ALICE Inner Tracking System (ITS): Technical Design Report*. Technical design report. ALICE. CERN, Geneva, 1999. <http://cds.cern.ch/record/391175>.
- [43] ALICE Collaboration, P. Cortese *et al.*, *ALICE technical design report on forward detectors: FMD, T0 and V0*. 9, 2004. <https://cds.cern.ch/record/781854>.
- [44] ALICE Collaboration, E. Abbas *et al.*, “Performance of the ALICE VZERO system”, *JINST* **8** (2013) P10016, arXiv:1306.3130 [nucl-ex].
- [45] ALICE Collaboration, “Centrality determination in heavy ion collisions.” ALICE-PUBLIC-2018-011, Aug., 2018. <http://cds.cern.ch/record/2636623>.
- [46] ALICE Collaboration, S. Acharya *et al.*, “Transverse momentum spectra and nuclear modification factors of charged particles in pp, p–Pb and Pb–Pb collisions at the LHC”, *JHEP* **11** (2018) 013, arXiv:1802.09145 [nucl-ex].
- [47] ALICE Collaboration, S. Acharya *et al.*, “Energy dependence and fluctuations of anisotropic flow in Pb–Pb collisions at $\sqrt{s_{\text{NN}}} = 5.02$ and 2.76 TeV”, *JHEP* **07** (2018) 103, arXiv:1804.02944 [nucl-ex].
- [48] ALICE Collaboration, “Supplemental material: Azimuthal anisotropy of jet particles in p–Pb and Pb–Pb collisions at $\sqrt{s_{\text{NN}}} = 5.02$ TeV”, ALICE-PUBLIC-2022-020 (Dec, 2022). <https://cds.cern.ch/record/2845233>.
- [49] ALICE Collaboration, S. Acharya *et al.*, “Measurements of azimuthal anisotropies at forward and backward rapidity with muons in high-multiplicity p–Pb collisions at $\sqrt{s_{\text{NN}}} = 8.16$ TeV”, *Phys. Lett. B* **846** (2023) 137782, arXiv:2210.08980 [nucl-ex].
- [50] ALICE Collaboration, B. Abelev *et al.*, “Long-range angular correlations on the near and away side in p–Pb collisions at $\sqrt{s_{\text{NN}}} = 5.02$ TeV”, *Phys. Lett. B* **719** (2013) 29–41, arXiv:1212.2001 [nucl-ex].
- [51] ALICE Collaboration, B. Abelev *et al.*, “Multiplicity dependence of jet-like two-particle correlation structures in p–Pb collisions at $\sqrt{s_{\text{NN}}} = 5.02$ TeV”, *Phys. Lett. B* **741** (2015) 38–50, arXiv:1406.5463 [nucl-ex].
- [52] ALICE Collaboration, J. Adam *et al.*, “Forward-central two-particle correlations in p–Pb collisions at $\sqrt{s_{\text{NN}}} = 5.02$ TeV”, *Phys. Lett. B* **753** (2016) 126–139, arXiv:1506.08032 [nucl-ex].

- [53] M. Luzum and J.-Y. Ollitrault, “Eliminating experimental bias in anisotropic-flow measurements of high-energy nuclear collisions”, *Phys. Rev. C* **87** (2013) 044907, arXiv:1209.2323 [nucl-ex].
- [54] ALICE Collaboration, S. Acharya *et al.*, “Measurements of long-range two-particle correlation over a wide pseudorapidity range in p–Pb collisions at $\sqrt{s_{\text{NN}}} = 5.0 \text{ TeV}$ ”, *JHEP* **01** (2024) 199, arXiv:2308.16590 [nucl-ex].
- [55] STAR Collaboration, C. Adler *et al.*, “Elliptic flow from two and four particle correlations in Au+Au collisions at $\sqrt{s_{\text{NN}}} = 130\text{-GeV}$ ”, *Phys. Rev. C* **66** (2002) 034904, arXiv:nucl-ex/0206001.
- [56] S. A. Voloshin, A. M. Poskanzer, and R. Snellings, “Collective phenomena in non-central nuclear collisions”, *Landolt-Bornstein* **23** (2010) 293–333, arXiv:0809.2949 [nucl-ex].
- [57] I. Selyuzhenkov and S. Voloshin, “Effects of non-uniform acceptance in anisotropic flow measurement”, *Phys. Rev. C* **77** (2008) 034904, arXiv:0707.4672 [nucl-th].
- [58] ALICE Collaboration, S. Acharya *et al.*, “Anisotropic flow of identified particles in Pb–Pb collisions at $\sqrt{s_{\text{NN}}} = 5.02 \text{ TeV}$ ”, *JHEP* **09** (2018) 006, arXiv:1805.04390 [nucl-ex].
- [59] ALICE Collaboration, E. Abbas *et al.*, “J/ ψ Elliptic Flow in Pb–Pb Collisions at $\sqrt{s_{\text{NN}}} = 2.76 \text{ TeV}$ ”, *Phys. Rev. Lett.* **111** (2013) 162301, arXiv:1303.5880 [nucl-ex].
- [60] Z.-W. Lin and L. Zheng, “Further developments of a multi-phase transport model for relativistic nuclear collisions”, *Nucl. Sci. Tech.* **32** (2021) 113, arXiv:2110.02989 [nucl-th].
- [61] C. Loizides, J. Kamin, and D. d’Enterria, “Improved Monte Carlo Glauber predictions at present and future nuclear colliders”, *Phys. Rev. C* **97** (2018) 054910, arXiv:1710.07098 [nucl-ex]. [Erratum: Phys.Rev.C 99, 019901 (2019)].
- [62] H.-S. Wang and G.-L. Ma, “Testing the collectivity in large and small colliding systems with test particles”, *Phys. Rev. C* **106** (2022) 064907, arXiv:2208.06854 [nucl-th].
- [63] X.-N. Wang and M. Gyulassy, “HIJING: A Monte Carlo model for multiple jet production in p p, p A and A A collisions”, *Phys. Rev. D* **44** (1991) 3501–3516.
- [64] M. Gyulassy and X.-N. Wang, “HIJING 1.0: A Monte Carlo program for parton and particle production in high-energy hadronic and nuclear collisions”, *Comput. Phys. Commun.* **83** (1994) 307, arXiv:nucl-th/9502021.
- [65] B. Zhang, “ZPC 1.0.1: A Parton cascade for ultrarelativistic heavy ion collisions”, *Comput. Phys. Commun.* **109** (1998) 193–206, arXiv:nucl-th/9709009.
- [66] B.-A. Li and C. M. Ko, “Formation of superdense hadronic matter in high-energy heavy ion collisions”, *Phys. Rev. C* **52** (1995) 2037–2063, arXiv:nucl-th/9505016.
- [67] S.-Y. Tang, L. Zheng, X.-M. Zhang, and R.-Z. Wan, “Investigating the elliptic anisotropy of identified particles in p–Pb collisions with a multi-phase transport model”, *Nucl. Sci. Tech.* **35** (2024) 32, arXiv:2303.06577 [hep-ph].
- [68] ALICE Collaboration, J. Adam *et al.*, “Multiplicity dependence of charged pion, kaon, and (anti)proton production at large transverse momentum in p–Pb collisions at $\sqrt{s_{\text{NN}}} = 5.02 \text{ TeV}$ ”, *Phys. Lett. B* **760** (2016) 720–735, arXiv:1601.03658 [nucl-ex].

A The ALICE Collaboration

- S. Acharya ¹²⁶, D. Adamová ⁸⁶, A. Adler ⁷⁰, G. Aglieri Rinella ³², M. Agnello ²⁹, N. Agrawal ⁵¹, Z. Ahammed ¹³⁴, S. Ahmad ¹⁵, S.U. Ahn ⁷¹, I. Ahuja ³⁷, A. Akindinov ¹⁴⁰, M. Al-Turany ⁹⁷, D. Aleksandrov ¹⁴⁰, B. Alessandro ⁵⁶, H.M. Alfanda ⁶, R. Alfaro Molina ⁶⁷, B. Ali ¹⁵, A. Alici ²⁵, N. Alizadehvandchali ¹¹⁵, A. Alkin ³², J. Alme ²⁰, G. Alocco ⁵², T. Alt ⁶⁴, I. Altsybeev ¹⁴⁰, J.R. Alvarado ⁴⁴, M.N. Anaam ⁶, C. Andrei ⁴⁵, A. Andronic ¹²⁵, V. Anguelov ⁹⁴, F. Antinori ⁵⁴, P. Antonioli ⁵¹, N. Apadula ⁷⁴, L. Aphecetche ¹⁰³, H. Appelshäuser ⁶⁴, C. Arata ⁷³, S. Arcelli ²⁵, M. Aresti ⁵², R. Arnaldi ⁵⁶, J.G.M.C.A. Arneiro ¹¹⁰, I.C. Arsene ¹⁹, M. Arslanbekov ¹³⁷, A. Augustinus ³², R. Averbeck ⁹⁷, M.D. Azmi ¹⁵, A. Badalà ⁵³, J. Bae ¹⁰⁴, Y.W. Baek ⁴⁰, X. Bai ¹¹⁹, R. Bailhache ⁶⁴, Y. Bailung ⁴⁸, A. Balbino ²⁹, A. Baldissari ¹²⁹, B. Balis ², D. Banerjee ⁴, Z. Banoo ⁹¹, R. Barbera ²⁶, F. Barile ³¹, L. Barioglio ⁹⁵, M. Barlou ⁷⁸, G.G. Barnaföldi ⁴⁶, L.S. Barnby ⁸⁵, V. Barret ¹²⁶, L. Barreto ¹¹⁰, C. Bartels ¹¹⁸, K. Barth ³², E. Bartsch ⁶⁴, N. Bastid ¹²⁶, S. Basu ⁷⁵, G. Batigne ¹⁰³, D. Battistini ⁹⁵, B. Batyunya ¹⁴¹, D. Bauri ⁴⁷, J.L. Bazo Alba ¹⁰¹, I.G. Bearden ⁸³, C. Beattie ¹³⁷, P. Becht ⁹⁷, D. Behera ⁴⁸, I. Belikov ¹²⁸, A.D.C. Bell Hechavarria ¹²⁵, F. Bellini ²⁵, R. Bellwied ¹¹⁵, S. Belokurova ¹⁴⁰, V. Belyaev ¹⁴⁰, G. Bencedi ⁴⁶, S. Beole ²⁴, Y. Berdnikov ¹⁴⁰, A. Berdnikova ⁹⁴, L. Bergmann ⁹⁴, M.G. Besiou ⁶³, L. Betev ³², P.P. Bhaduri ¹³⁴, A. Bhasin ⁹¹, M.A. Bhat ⁴, B. Bhattacharjee ⁴¹, L. Bianchi ²⁴, N. Bianchi ⁴⁹, J. Bielčík ³⁵, J. Bielčíková ⁸⁶, J. Biernat ¹⁰⁷, A.P. Bigot ¹²⁸, A. Bilandzic ⁹⁵, G. Biro ⁴⁶, S. Biswas ⁴, N. Bize ¹⁰³, J.T. Blair ¹⁰⁸, D. Blau ¹⁴⁰, M.B. Blidaru ⁹⁷, N. Bluhme ³⁸, C. Blume ⁶⁴, G. Boca ^{21,55}, F. Bock ⁸⁷, T. Bodova ²⁰, A. Bogdanov ¹⁴⁰, S. Boi ²², J. Bok ⁵⁸, L. Boldizsár ⁴⁶, M. Bombara ³⁷, P.M. Bond ³², G. Bonomi ^{133,55}, H. Borel ¹²⁹, A. Borissov ¹⁴⁰, A.G. Borquez Carcamo ⁹⁴, H. Bossi ¹³⁷, E. Botta ²⁴, Y.E.M. Bouziani ⁶⁴, L. Bratrud ⁶⁴, P. Braun-Munzinger ⁹⁷, M. Bregant ¹¹⁰, M. Broz ³⁵, G.E. Bruno ^{96,31}, M.D. Buckland ²³, D. Budnikov ¹⁴⁰, H. Buesching ⁶⁴, S. Bufalino ²⁹, O. Bugnon ¹⁰³, P. Buhler ¹⁰², Z. Buthelezi ^{68,122}, S.A. Bysiak ¹⁰⁷, M. Cai ⁶, H. Caines ¹³⁷, A. Caliva ⁹⁷, E. Calvo Villar ¹⁰¹, J.M.M. Camacho ¹⁰⁹, P. Camerini ²³, F.D.M. Canedo ¹¹⁰, S.L. Cantway ¹³⁷, M. Carabas ¹¹³, A.A. Carballo ³², F. Carnesecchi ³², R. Caron ¹²⁷, L.A.D. Carvalho ¹¹⁰, J. Castillo Castellanos ¹²⁹, F. Catalano ²⁴, C. Ceballos Sanchez ¹⁴¹, I. Chakaberia ⁷⁴, P. Chakraborty ⁴⁷, S. Chandra ¹³⁴, S. Chapeland ³², M. Chartier ¹¹⁸, S. Chattopadhyay ¹³⁴, S. Chattopadhyay ⁹⁹, T. Cheng ^{97,6}, C. Cheshkov ¹²⁷, B. Cheynis ¹²⁷, V. Chibante Barroso ³², D.D. Chinellato ¹¹¹, E.S. Chizzali ^{II,95}, J. Cho ⁵⁸, S. Cho ⁵⁸, P. Chochula ³², P. Christakoglou ⁸⁴, C.H. Christensen ⁸³, P. Christiansen ⁷⁵, T. Chujo ¹²⁴, M. Ciaccio ²⁹, C. Ciccalo ⁵², F. Cindolo ⁵¹, M.R. Ciupek ⁹⁷, G. Clai ^{III,51}, F. Colamaria ⁵⁰, J.S. Colburn ¹⁰⁰, D. Colella ^{96,31}, M. Colocci ²⁵, M. Concas ⁵⁶, G. Conesa Balbastre ⁷³, Z. Conesa del Valle ¹³⁰, G. Contin ²³, J.G. Contreras ³⁵, M.L. Coquet ¹²⁹, T.M. Cormier ^{I,87}, P. Cortese ^{132,56}, M.R. Cosentino ¹¹², F. Costa ³², S. Costanza ^{21,55}, C. Cot ¹³⁰, J. Crkovská ⁹⁴, P. Crochet ¹²⁶, R. Cruz-Torres ⁷⁴, E. Cuautle ⁶⁵, P. Cui ⁶, A. Dainese ⁵⁴, M.C. Danisch ⁹⁴, A. Danu ⁶³, P. Das ⁸⁰, P. Das ⁴, S. Das ⁴, A.R. Dash ¹²⁵, S. Dash ⁴⁷, A. De Caro ²⁸, G. de Cataldo ⁵⁰, J. de Cuveland ³⁸, A. De Falco ²², D. De Gruttola ²⁸, N. De Marco ⁵⁶, C. De Martin ²³, S. De Pasquale ²⁸, R. Deb ¹³³, S. Deb ⁴⁸, R.J. Debski ², K.R. Deja ¹³⁵, R. Del Grande ⁹⁵, L. Dello Stritto ²⁸, W. Deng ⁶, P. Dhankher ¹⁸, D. Di Bari ³¹, A. Di Mauro ³², R.A. Diaz ^{141,7}, T. Dietel ¹¹⁴, Y. Ding ^{127,6}, R. Divià ³², D.U. Dixit ¹⁸, Ø. Djupsland ²⁰, U. Dmitrieva ¹⁴⁰, A. Dobrin ⁶³, B. Dönigus ⁶⁴, J.M. Dubinski ¹³⁵, A. Dubla ⁹⁷, S. Dudi ⁹⁰, P. Dupieux ¹²⁶, M. Durkac ¹⁰⁶, N. Dzalaiova ¹², T.M. Eder ¹²⁵, R.J. Ehlers ⁸⁷, V.N. Eikeland ²⁰, F. Eisenhut ⁶⁴, D. Elia ⁵⁰, B. Erazmus ¹⁰³, F. Ercolossi ²⁵, F. Erhardt ⁸⁹, M.R. Ersdal ²⁰, B. Espagnon ¹³⁰, G. Eulisse ³², D. Evans ¹⁰⁰, S. Evdokimov ¹⁴⁰, L. Fabbietti ⁹⁵, M. Faggin ²⁷, J. Faivre ⁷³, F. Fan ⁶, W. Fan ⁷⁴, A. Fantoni ⁴⁹, M. Fasel ⁸⁷, P. Fecchio ²⁹, A. Feliciello ⁵⁶, G. Feofilov ¹⁴⁰, A. Fernández Téllez ⁴⁴, L. Ferrandi ¹¹⁰, M.B. Ferrer ³², A. Ferrero ¹²⁹, C. Ferrero ^{IV,56}, A. Ferretti ²⁴, V.J.G. Feuillard ⁹⁴, V. Filova ³⁵, D. Finogeev ¹⁴⁰, F.M. Fionda ⁵², F. Flor ¹¹⁵, A.N. Flores ¹⁰⁸, S. Foertsch ⁶⁸, I. Fokin ⁹⁴, S. Fokin ¹⁴⁰, E. Fragiocomo ⁵⁷, E. Frajna ⁴⁶, U. Fuchs ³², N. Funicello ²⁸, C. Furret ⁷³, A. Furs ¹⁴⁰, T. Fusayasu ⁹⁸, J.J. Gaardhøje ⁸³, M. Gagliardi ²⁴, A.M. Gago ¹⁰¹, C.D. Galvan ¹⁰⁹, D.R. Gangadharan ¹¹⁵, P. Ganoti ⁷⁸, C. Garabatos ⁹⁷, T. García Chávez ⁴⁴, E. Garcia-Solis ⁹, K. Garg ¹⁰³, C. Gargiulo ³², K. Garner ¹²⁵, P. Gasik ⁹⁷, A. Gautam ¹¹⁷, M.B. Gay Ducati ⁶⁶, M. Germain ¹⁰³, A. Ghimouz ¹²⁴, C. Ghosh ¹³⁴, M. Giacalone ^{51,25}, P. Giubellino ^{97,56}, P. Giubilato ²⁷, A.M.C. Glaenzer ¹²⁹, P. Glässel ⁹⁴, E. Glimos ¹²¹, D.J.Q. Goh ⁷⁶, V. Gonzalez ¹³⁶, L.H. González-Trueba ⁶⁷, M. Gorgon ², S. Gotovac ³³, V. Grabski ⁶⁷, L.K. Graczykowski ¹³⁵, E. Grecka ⁸⁶, A. Grelli ⁵⁹, C. Grigoras ³², V. Grigoriev ¹⁴⁰, S. Grigoryan ^{141,1}, F. Grossa ³², J.F. Grosse-Oetringhaus ³², R. Grossi ⁹⁷, D. Grund ³⁵, G.G. Guardiano ¹¹¹, R. Guernane ⁷³, M. Guilbaud ¹⁰³, K. Gulbrandsen ⁸³, T. Gündem ⁶⁴, T. Gunji ¹²³, W. Guo ⁶,

- A. Gupta ⁹¹, R. Gupta ⁹¹, L. Gyulai ⁴⁶, M.K. Habib⁹⁷, C. Hadjidakis ¹³⁰, F.U. Haider ⁹¹, H. Hamagaki ⁷⁶, A. Hamdi ⁷⁴, M. Hamid⁶, Y. Han ¹³⁸, R. Hannigan ¹⁰⁸, M.R. Haque ¹³⁵, J.W. Harris ¹³⁷, A. Harton ⁹, H. Hassan ⁸⁷, D. Hatzifotiadou ⁵¹, P. Hauer ⁴², L.B. Havener ¹³⁷, S.T. Heckel ⁹⁵, E. Hellbär ⁹⁷, H. Helstrup ³⁴, M. Hemmer ⁶⁴, T. Herman ³⁵, G. Herrera Corral ⁸, F. Herrmann ¹²⁵, S. Herrmann ¹²⁷, K.F. Hetland ³⁴, B. Heybeck ⁶⁴, H. Hillemanns ³², C. Hills ¹¹⁸, B. Hippolyte ¹²⁸, F.W. Hoffmann ⁷⁰, B. Hofman ⁵⁹, B. Hohlweber ⁸⁴, G.H. Hong ¹³⁸, M. Horst ⁹⁵, A. Horzyk ², Y. Hou ⁶, P. Hristov ³², C. Hughes ¹²¹, P. Huhn ⁶⁴, L.M. Huhta ¹¹⁶, T.J. Humanic ⁸⁸, A. Hutson ¹¹⁵, D. Hutter ³⁸, J.P. Iddon ¹¹⁸, R. Ilkaev ¹⁴⁰, H. Ilyas ¹³, M. Inaba ¹²⁴, G.M. Innocenti ³², M. Ippolitov ¹⁴⁰, A. Isakov ⁸⁶, T. Isidori ¹¹⁷, M.S. Islam ⁹⁹, M. Ivanov ⁹⁷, M. Ivanov ¹², V. Ivanov ¹⁴⁰, M. Jablonski ², B. Jacak ⁷⁴, N. Jacazio ³², P.M. Jacobs ⁷⁴, S. Jadlovska ¹⁰⁶, J. Jadlovsky ¹⁰⁶, S. Jaelani ⁸², L. Jaffe ³⁸, C. Jahnke ¹¹¹, M.J. Jakubowska ¹³⁵, M.A. Janik ¹³⁵, T. Janson ⁷⁰, M. Jercic ⁸⁹, S. Jia ¹⁰, A.A.P. Jimenez ⁶⁵, F. Jonas ^{87,125}, J.M. Jowett ^{32,97}, J. Jung ⁶⁴, M. Jung ⁶⁴, A. Junique ³², A. Jusko ¹⁰⁰, J. Kaewjai ¹⁰⁵, P. Kalinak ⁶⁰, A.S. Kalteyer ⁹⁷, A. Kalweit ³², V. Kaplin ¹⁴⁰, A. Karasu Uysal ^{V,72}, D. Karatovic ⁸⁹, O. Karavichev ¹⁴⁰, T. Karavicheva ¹⁴⁰, P. Karczmarczyk ¹³⁵, E. Karpechev ¹⁴⁰, M.J. Karwowska ^{32,135}, U. Kebschull ⁷⁰, R. Keidel ¹³⁹, D.L.D. Keijdener ⁵⁹, M. Keil ³², B. Ketzer ⁴², A.M. Khan ⁶, S. Khan ¹⁵, A. Khanzadeev ¹⁴⁰, Y. Kharlov ¹⁴⁰, A. Khatun ^{117,15}, A. Khuntia ¹⁰⁷, M.B. Kidson ¹¹⁴, B. Kileng ³⁴, B. Kim ¹⁶, C. Kim ¹⁶, D.J. Kim ¹¹⁶, E.J. Kim ⁶⁹, J. Kim ¹³⁸, J.S. Kim ⁴⁰, J. Kim ⁶⁹, M. Kim ^{18,94}, S. Kim ¹⁷, T. Kim ¹³⁸, K. Kimura ⁹², S. Kirsch ⁶⁴, I. Kisel ³⁸, S. Kiselev ¹⁴⁰, A. Kisiel ¹³⁵, J.P. Kitowski ², J.L. Klay ⁵, J. Klein ³², S. Klein ⁷⁴, C. Klein-Bösing ¹²⁵, M. Kleiner ⁶⁴, T. Klemenz ⁹⁵, A. Kluge ³², A.G. Knospe ¹¹⁵, C. Kobdaj ¹⁰⁵, T. Kollegger ⁹⁷, A. Kondratyev ¹⁴¹, N. Kondratyeva ¹⁴⁰, E. Kondratyuk ¹⁴⁰, J. Konig ⁶⁴, S.A. Konigstorfer ⁹⁵, P.J. Konopka ³², G. Kornakov ¹³⁵, M. Korwieser ⁹⁵, S.D. Koryciak ², A. Kotliarov ⁸⁶, V. Kovalenko ¹⁴⁰, M. Kowalski ¹⁰⁷, V. Kozhuharov ³⁶, I. Králik ⁶⁰, A. Kravčáková ³⁷, L. Krcal ^{32,38}, L. Kreis ⁹⁷, M. Krivda ^{100,60}, F. Krizek ⁸⁶, K. Krizkova Gajdosova ³⁵, M. Kroesen ⁹⁴, M. Krüger ⁶⁴, D.M. Krupova ³⁵, E. Kryshen ¹⁴⁰, V. Kučera ³², C. Kuhn ¹²⁸, P.G. Kuijer ⁸⁴, T. Kumaoka ¹²⁴, D. Kumar ¹³⁴, L. Kumar ⁹⁰, N. Kumar ⁹⁰, S. Kumar ³¹, S. Kundu ³², P. Kurashvili ⁷⁹, A. Kurepin ¹⁴⁰, A.B. Kurepin ¹⁴⁰, A. Kuryakin ¹⁴⁰, S. Kushpil ⁸⁶, J. Kvapil ¹⁰⁰, M.J. Kweon ⁵⁸, J.Y. Kwon ⁵⁸, Y. Kwon ¹³⁸, S.L. La Pointe ³⁸, P. La Rocca ²⁶, Y.S. Lai ⁷⁴, A. Lakrathok ¹⁰⁵, M. Lamanna ³², R. Langoy ¹²⁰, P. Larionov ³², E. Laudi ³², L. Lautner ^{32,95}, R. Lavicka ¹⁰², T. Lazareva ¹⁴⁰, R. Lea ^{133,55}, H. Lee ¹⁰⁴, G. Legras ¹²⁵, J. Lehrbach ³⁸, T.M. Lelek ², R.C. Lemmon ⁸⁵, I. León Monzón ¹⁰⁹, M.M. Lesch ⁹⁵, E.D. Lesser ¹⁸, M. Lettrich ⁹⁵, P. Lévai ⁴⁶, X. Li ¹⁰, X.L. Li ⁶, J. Lien ¹²⁰, R. Lietava ¹⁰⁰, I. Likmeta ¹¹⁵, B. Lim ^{24,16}, S.H. Lim ¹⁶, V. Lindenstruth ³⁸, A. Lindner ⁴⁵, C. Lippmann ⁹⁷, A. Liu ¹⁸, D.H. Liu ⁶, J. Liu ¹¹⁸, I.M. Lofnes ²⁰, C. Loizides ⁸⁷, S. Lokos ¹⁰⁷, J. Lömker ⁵⁹, P. Loncar ³³, J.A. Lopez ⁹⁴, X. Lopez ¹²⁶, E. López Torres ⁷, P. Lu ^{97,119}, J.R. Luhder ¹²⁵, M. Lunardon ²⁷, G. Luparello ⁵⁷, Y.G. Ma ³⁹, A. Maevskaya ¹⁴⁰, M. Mager ³², T. Mahmoud ⁴², A. Maire ¹²⁸, M.V. Makariev ³⁶, M. Malaev ¹⁴⁰, G. Malfattore ²⁵, N.M. Malik ⁹¹, Q.W. Malik ¹⁹, S.K. Malik ⁹¹, L. Malinina ^{I,VIII,141}, D. Mal'Kevich ¹⁴⁰, D. Mallick ⁸⁰, N. Mallick ⁴⁸, G. Mandaglio ^{30,53}, S.K. Mandal ⁷⁹, V. Manko ¹⁴⁰, F. Manso ¹²⁶, V. Manzari ⁵⁰, Y. Mao ⁶, G.V. Margagliotti ²³, A. Margotti ⁵¹, A. Marín ⁹⁷, C. Markert ¹⁰⁸, P. Martinengo ³², J.L. Martinez ¹¹⁵, M.I. Martínez ⁴⁴, G. Martínez García ¹⁰³, S. Masciocchi ⁹⁷, M. Masera ²⁴, A. Masoni ⁵², L. Massacrier ¹³⁰, A. Mastroserio ^{131,50}, O. Matonoha ⁷⁵, P.F.T. Matuoka ¹¹⁰, A. Matyja ¹⁰⁷, C. Mayer ¹⁰⁷, A.L. Mazuecos ³², F. Mazzaschi ²⁴, M. Mazzilli ³², J.E. Mdhului ¹²², A.F. Mechler ⁶⁴, Y. Melikyan ^{43,140}, A. Menchaca-Rocha ⁶⁷, E. Meninno ¹⁰², A.S. Menon ¹¹⁵, M. Meres ¹², S. Mhlanga ^{114,68}, Y. Miake ¹²⁴, L. Micheletti ⁵⁶, L.C. Migliorin ¹²⁷, D.L. Miyaylov ⁹⁵, K. Mikhaylov ^{141,140}, A.N. Mishra ⁴⁶, D. Miśkowiec ⁹⁷, A. Modak ⁴, A.P. Mohanty ⁵⁹, B. Mohanty ⁸⁰, M. Mohisin Khan ^{VI,15}, M.A. Molander ⁴³, Z. Moravcova ⁸³, C. Mordasini ⁹⁵, D.A. Moreira De Godoy ¹²⁵, I. Morozov ¹⁴⁰, A. Morsch ³², T. Mrnjavac ³², V. Muccifora ⁴⁹, S. Muhuri ¹³⁴, J.D. Mulligan ⁷⁴, A. Mulliri ²², M.G. Munhoz ¹¹⁰, R.H. Munzer ⁶⁴, H. Murakami ¹²³, S. Murray ¹¹⁴, L. Musa ³², J. Musinsky ⁶⁰, J.W. Myrcha ¹³⁵, B. Naik ¹²², A.I. Nambrath ¹⁸, B.K. Nandi ⁴⁷, R. Nania ⁵¹, E. Nappi ⁵⁰, A.F. Nassirpour ⁷⁵, A. Nath ⁹⁴, C. Natrass ¹²¹, M.N. Naydenov ³⁶, A. Neagu ¹⁹, A. Negru ¹¹³, L. Nellen ⁶⁵, S.V. Nesbo ³⁴, G. Neskovic ³⁸, D. Nesterov ¹⁴⁰, B.S. Nielsen ⁸³, E.G. Nielsen ⁸³, S. Nikolaev ¹⁴⁰, S. Nikulin ¹⁴⁰, V. Nikulin ¹⁴⁰, F. Noferini ⁵¹, S. Noh ¹¹, P. Nomokonov ¹⁴¹, J. Norman ¹¹⁸, N. Novitzky ¹²⁴, P. Nowakowski ¹³⁵, A. Nyandin ¹⁴⁰, J. Nystrand ²⁰, M. Ogino ⁷⁶, A. Ohlson ⁷⁵, V.A. Okorokov ¹⁴⁰, J. Oleniacz ¹³⁵, A.C. Oliveira Da Silva ¹²¹, M.H. Oliver ¹³⁷, A. Onnerstad ¹¹⁶, C. Oppedisano ⁵⁶, A. Ortiz Velasquez ⁶⁵, J. Otwinowski ¹⁰⁷, M. Oya ⁹², K. Oyama ⁷⁶, Y. Pachmayer ⁹⁴, S. Padhan ⁴⁷, D. Pagano ^{133,55}, G. Paić ⁶⁵, S. Paisano-Guzmán ⁴⁴, A. Palasciano ⁵⁰,

- S. Panebianco ¹²⁹, H. Park ¹²⁴, H. Park ¹⁰⁴, J. Park ⁵⁸, J.E. Parkkila ³², R.N. Patra ⁹¹, B. Paul ²², H. Pei ⁶, T. Peitzmann ⁵⁹, X. Peng ⁶, M. Pennisi ²⁴, L.G. Pereira ⁶⁶, D. Peresunko ¹⁴⁰, G.M. Perez ⁷, S. Perrin ¹²⁹, Y. Pestov ¹⁴⁰, V. Petráček ³⁵, V. Petrov ¹⁴⁰, M. Petrovici ⁴⁵, R.P. Pezzi ^{103,66}, S. Piano ⁵⁷, M. Pikna ¹², P. Pillot ¹⁰³, O. Pinazza ^{51,32}, L. Pinsky ¹¹⁵, C. Pinto ⁹⁵, S. Pisano ⁴⁹, M. Płoskoń ⁷⁴, M. Planinic ⁸⁹, F. Pliquet ⁶⁴, M.G. Poghosyan ⁸⁷, B. Polichtchouk ¹⁴⁰, S. Politano ²⁹, N. Poljak ⁸⁹, A. Pop ⁴⁵, S. Porteboeuf-Houssais ¹²⁶, V. Pozdniakov ¹⁴¹, K.K. Pradhan ⁴⁸, S.K. Prasad ⁴, S. Prasad ⁴⁸, R. Preghenella ⁵¹, F. Prino ⁵⁶, C.A. Pruneau ¹³⁶, I. Pshenichnov ¹⁴⁰, M. Puccio ³², S. Pucillo ²⁴, Z. Pugelova ¹⁰⁶, S. Qiu ⁸⁴, L. Quaglia ²⁴, R.E. Quishpe ¹¹⁵, S. Ragoni ¹⁴, A. Rakotozafindrabe ¹²⁹, L. Ramello ^{132,56}, F. Rami ¹²⁸, T.A. Rancien ⁷³, M. Rasa ²⁶, S.S. Räsänen ⁴³, R. Rath ⁵¹, M.P. Rauch ²⁰, I. Ravasenga ⁸⁴, K.F. Read ^{87,121}, C. Reckziegel ¹¹², A.R. Redelbach ³⁸, K. Redlich ^{VII,79}, C.A. Reetz ⁹⁷, H.D. Regules-Medel ⁴⁴, A. Rehman ²⁰, F. Reidt ³², H.A. Reme-Ness ³⁴, Z. Rescakova ³⁷, K. Reygers ⁹⁴, A. Riabov ¹⁴⁰, V. Riabov ¹⁴⁰, R. Ricci ²⁸, M. Richter ¹⁹, A.A. Riedel ⁹⁵, W. Riegler ³², C. Ristea ⁶³, M. Rodríguez Cahuantzi ⁴⁴, S.A. Rodríguez Ramírez ⁴⁴, K. Røed ¹⁹, R. Rogalev ¹⁴⁰, E. Rogochaya ¹⁴¹, T.S. Rogoschinski ⁶⁴, D. Rohr ³², D. Röhrlrich ²⁰, P.F. Rojas ⁴⁴, S. Rojas Torres ³⁵, P.S. Rokita ¹³⁵, G. Romanenko ¹⁴¹, F. Ronchetti ⁴⁹, A. Rosano ^{30,53}, E.D. Rosas ⁶⁵, K. Roslon ¹³⁵, A. Rossi ⁵⁴, A. Roy ⁴⁸, S. Roy ⁴⁷, N. Rubini ²⁵, D. Ruggiano ¹³⁵, R. Rui ²³, B. Rumyantsev ¹⁴¹, P.G. Russek ², R. Russo ⁸⁴, A. Rustamov ⁸¹, E. Ryabinkin ¹⁴⁰, Y. Ryabov ¹⁴⁰, A. Rybicki ¹⁰⁷, H. Rytkonen ¹¹⁶, W. Rzesz ¹³⁵, O.A.M. Saarimaki ⁴³, R. Sadek ¹⁰³, S. Sadhu ³¹, S. Sadovsky ¹⁴⁰, J. Saetre ²⁰, K. Šafářík ³⁵, S.K. Saha ⁴, S. Saha ⁸⁰, B. Sahoo ⁴⁷, R. Sahoo ⁴⁸, S. Sahoo ⁶¹, D. Sahu ⁴⁸, P.K. Sahu ⁶¹, J. Saini ¹³⁴, K. Sajdakova ³⁷, S. Sakai ¹²⁴, M.P. Salvan ⁹⁷, S. Sambyal ⁹¹, I. Sanna ^{32,95}, T.B. Saramela ¹¹⁰, D. Sarkar ¹³⁶, N. Sarkar ¹³⁴, P. Sarma ⁴¹, V. Sarritzu ²², V.M. Sarti ⁹⁵, M.H.P. Sas ¹³⁷, J. Schambach ⁸⁷, H.S. Scheid ⁶⁴, C. Schiaua ⁴⁵, R. Schicker ⁹⁴, A. Schmah ⁹⁴, C. Schmidt ⁹⁷, H.R. Schmidt ⁹³, M.O. Schmidt ³², M. Schmidt ⁹³, N.V. Schmidt ⁸⁷, A.R. Schmier ¹²¹, R. Schotter ¹²⁸, A. Schröter ³⁸, J. Schukraft ³², K. Schwarz ⁹⁷, K. Schweda ⁹⁷, G. Scioli ²⁵, E. Scomparin ⁵⁶, J.E. Seger ¹⁴, Y. Sekiguchi ¹²³, D. Sekihata ¹²³, I. Selyuzhenkov ^{97,140}, S. Senyukov ¹²⁸, J.J. Seo ⁵⁸, D. Serebryakov ¹⁴⁰, L. Šerkšnytė ⁹⁵, A. Sevcenco ⁶³, T.J. Shaba ⁶⁸, A. Shabetai ¹⁰³, R. Shahoyan ³², A. Shangaraev ¹⁴⁰, A. Sharma ⁹⁰, B. Sharma ⁹¹, D. Sharma ⁴⁷, H. Sharma ¹⁰⁷, M. Sharma ⁹¹, S. Sharma ⁷⁶, S. Sharma ⁹¹, U. Sharma ⁹¹, A. Shatat ¹³⁰, O. Sheibani ¹¹⁵, K. Shigaki ⁹², M. Shimomura ⁷⁷, J. Shin ¹¹, S. Shirinkin ¹⁴⁰, Q. Shou ³⁹, Y. Sibiriak ¹⁴⁰, S. Siddhanta ⁵², T. Siemianczuk ⁷⁹, T.F. Silva ¹¹⁰, D. Silvermyr ⁷⁵, T. Simantathammakul ¹⁰⁵, R. Simeonov ³⁶, B. Singh ⁹¹, B. Singh ⁹⁵, R. Singh ⁸⁰, R. Singh ⁹¹, R. Singh ⁴⁸, S. Singh ¹⁵, V.K. Singh ¹³⁴, V. Singhal ¹³⁴, T. Sinha ⁹⁹, B. Sitar ¹², M. Sitta ^{132,56}, T.B. Skaali ¹⁹, G. Skorodumovs ⁹⁴, M. Slupecki ⁴³, N. Smirnov ¹³⁷, R.J.M. Snellings ⁵⁹, E.H. Solheim ¹⁹, J. Song ¹¹⁵, A. Songmoolnak ¹⁰⁵, F. Soramel ²⁷, R. Spijkers ⁸⁴, I. Sputowska ¹⁰⁷, J. Staa ⁷⁵, J. Stachel ⁹⁴, I. Stan ⁶³, P.J. Steffanic ¹²¹, S.F. Stiefelmaier ⁹⁴, D. Stocco ¹⁰³, I. Storehaug ¹⁹, P. Stratmann ¹²⁵, S. Strazzi ²⁵, C.P. Stylianidis ⁸⁴, A.A.P. Suaide ¹¹⁰, C. Suire ¹³⁰, M. Sukhanov ¹⁴⁰, M. Suljic ³², R. Sultanov ¹⁴⁰, V. Sumberia ⁹¹, S. Sumowidagdo ⁸², S. Swain ⁶¹, I. Szarka ¹², M. Szymkowski ¹³⁵, S.F. Taghavi ⁹⁵, G. Taillepied ⁹⁷, J. Takahashi ¹¹¹, G.J. Tambave ²⁰, S. Tang ^{126,6}, Z. Tang ¹¹⁹, J.D. Tapia Takaki ¹¹⁷, N. Tapus ¹¹³, L.A. Tarasovicova ¹²⁵, M.G. Tarzila ⁴⁵, G.F. Tassielli ³¹, A. Tauro ³², G. Tejeda Muñoz ⁴⁴, A. Telesca ³², L. Terlizzi ²⁴, C. Terrevoli ¹¹⁵, G. Tersimonov ³, S. Thakur ⁴, D. Thomas ¹⁰⁸, A. Tikhonov ¹⁴⁰, A.R. Timmins ¹¹⁵, M. Tkacik ¹⁰⁶, T. Tkacik ¹⁰⁶, A. Toia ⁶⁴, R. Tokumoto ⁹², N. Topilskaya ¹⁴⁰, M. Toppi ⁴⁹, F. Torales-Acosta ¹⁸, T. Tork ¹³⁰, A.G. Torres Ramos ³¹, A. Trifiró ^{30,53}, A.S. Triolo ^{30,53}, S. Tripathy ⁵¹, T. Tripathy ⁴⁷, S. Trogolo ³², V. Trubnikov ³, W.H. Trzaska ¹¹⁶, T.P. Trzciński ¹³⁵, A. Tumkin ¹⁴⁰, R. Turrisi ⁵⁴, T.S. Tveter ¹⁹, K. Ullaland ²⁰, B. Ulukutlu ⁹⁵, A. Uras ¹²⁷, M. Urioni ^{55,133}, G.L. Usai ²², M. Vala ³⁷, N. Valle ²¹, L.V.R. van Doremalen ⁵⁹, C. Van Hulse ¹³⁰, M. van Leeuwen ⁸⁴, C.A. van Veen ⁹⁴, R.J.G. van Weelden ⁸⁴, P. Vande Vyvre ³², D. Varga ⁴⁶, Z. Varga ⁴⁶, M. Vasileiou ⁷⁸, A. Vasiliev ¹⁴⁰, O. Vázquez Doce ⁴⁹, O. Vazquez Rueda ^{115,75}, V. Vechernin ¹⁴⁰, E. Vercellin ²⁴, S. Vergara Limón ⁴⁴, L. Vermunt ⁹⁷, R. Vértesi ⁴⁶, M. Verweij ⁵⁹, L. Vickovic ³³, Z. Vilakazi ¹²², O. Villalobos Baillie ¹⁰⁰, A. Villani ²³, G. Vino ⁵⁰, A. Vinogradov ¹⁴⁰, T. Virgili ²⁸, M.M.O. Virta ¹¹⁶, V. Vislavicius ⁷⁵, A. Vodopyanov ¹⁴¹, B. Volkel ³², M.A. Völkli ⁹⁴, K. Voloshin ¹⁴⁰, S.A. Voloshin ¹³⁶, G. Volpe ³¹, B. von Haller ³², I. Vorobyev ⁹⁵, N. Vozniuk ¹⁴⁰, J. Vrláková ³⁷, C. Wang ³⁹, D. Wang ³⁹, Y. Wang ³⁹, A. Wegrzynek ³², F.T. Weighofer ³⁸, S.C. Wenzel ³², J.P. Wessels ¹²⁵, J. Wiechula ⁶⁴, J. Wikne ¹⁹, G. Wilk ⁷⁹, J. Wilkinson ⁹⁷, G.A. Willems ¹²⁵, B. Windelband ⁹⁴, M. Winn ¹²⁹, J.R. Wright ¹⁰⁸, W. Wu ³⁹, Y. Wu ¹¹⁹, R. Xu ⁶, A. Yadav ⁴², A.K. Yadav ¹³⁴, S. Yalcin ⁷², Y. Yamaguchi ⁹², S. Yang ²⁰, S. Yano ⁹², Z. Yin ⁶, I.-K. Yoo ¹⁶, J.H. Yoon ⁵⁸, S. Yuan ²⁰, A. Yuncu ⁹⁴, V. Zaccole ²³, C. Zampolli ³², F. Zanone ⁹⁴, N. Zardoshti ^{32,100}, A. Zarochentsev ¹⁴⁰, P. Závada ⁶²,

N. Zaviyalov¹⁴⁰, M. Zhalov¹⁴⁰, B. Zhang¹⁴⁰⁶, L. Zhang¹⁴⁰³⁹, M. Zhang⁶, S. Zhang¹⁴⁰³⁹, X. Zhang¹⁴⁰⁶, Y. Zhang¹¹⁹, Z. Zhang¹⁴⁰⁶, M. Zhao¹⁴⁰¹⁰, V. Zherebchevskii¹⁴⁰, Y. Zhi¹⁰, D. Zhou¹⁴⁰⁶, Y. Zhou¹⁴⁰⁸³, J. Zhu¹⁴⁰^{97,6}, Y. Zhu⁶, S.C. Zugravel¹⁴⁰⁵⁶, N. Zurlo¹⁴⁰^{133,55}

Affiliation Notes

^I Deceased

^{II} Also at: Max-Planck-Institut fur Physik, Munich, Germany

^{III} Also at: Italian National Agency for New Technologies, Energy and Sustainable Economic Development (ENEA), Bologna, Italy

^{IV} Also at: Dipartimento DET del Politecnico di Torino, Turin, Italy

^V Also at: Yildiz Technical University, Istanbul, Türkiye

^{VI} Also at: Department of Applied Physics, Aligarh Muslim University, Aligarh, India

^{VII} Also at: Institute of Theoretical Physics, University of Wroclaw, Poland

^{VIII} Also at: An institution covered by a cooperation agreement with CERN

Collaboration Institutes

¹ A.I. Alikhanyan National Science Laboratory (Yerevan Physics Institute) Foundation, Yerevan, Armenia

² AGH University of Krakow, Cracow, Poland

³ Bogolyubov Institute for Theoretical Physics, National Academy of Sciences of Ukraine, Kiev, Ukraine

⁴ Bose Institute, Department of Physics and Centre for Astroparticle Physics and Space Science (CAPSS), Kolkata, India

⁵ California Polytechnic State University, San Luis Obispo, California, United States

⁶ Central China Normal University, Wuhan, China

⁷ Centro de Aplicaciones Tecnológicas y Desarrollo Nuclear (CEADEN), Havana, Cuba

⁸ Centro de Investigación y de Estudios Avanzados (CINVESTAV), Mexico City and Mérida, Mexico

⁹ Chicago State University, Chicago, Illinois, United States

¹⁰ China Institute of Atomic Energy, Beijing, China

¹¹ Chungbuk National University, Cheongju, Republic of Korea

¹² Comenius University Bratislava, Faculty of Mathematics, Physics and Informatics, Bratislava, Slovak Republic

¹³ COMSATS University Islamabad, Islamabad, Pakistan

¹⁴ Creighton University, Omaha, Nebraska, United States

¹⁵ Department of Physics, Aligarh Muslim University, Aligarh, India

¹⁶ Department of Physics, Pusan National University, Pusan, Republic of Korea

¹⁷ Department of Physics, Sejong University, Seoul, Republic of Korea

¹⁸ Department of Physics, University of California, Berkeley, California, United States

¹⁹ Department of Physics, University of Oslo, Oslo, Norway

²⁰ Department of Physics and Technology, University of Bergen, Bergen, Norway

²¹ Dipartimento di Fisica, Università di Pavia, Pavia, Italy

²² Dipartimento di Fisica dell’Università and Sezione INFN, Cagliari, Italy

²³ Dipartimento di Fisica dell’Università and Sezione INFN, Trieste, Italy

²⁴ Dipartimento di Fisica dell’Università and Sezione INFN, Turin, Italy

²⁵ Dipartimento di Fisica e Astronomia dell’Università and Sezione INFN, Bologna, Italy

²⁶ Dipartimento di Fisica e Astronomia dell’Università and Sezione INFN, Catania, Italy

²⁷ Dipartimento di Fisica e Astronomia dell’Università and Sezione INFN, Padova, Italy

²⁸ Dipartimento di Fisica ‘E.R. Caianiello’ dell’Università and Gruppo Collegato INFN, Salerno, Italy

²⁹ Dipartimento DISAT del Politecnico and Sezione INFN, Turin, Italy

³⁰ Dipartimento di Scienze MIFT, Università di Messina, Messina, Italy

³¹ Dipartimento Interateneo di Fisica ‘M. Merlin’ and Sezione INFN, Bari, Italy

³² European Organization for Nuclear Research (CERN), Geneva, Switzerland

³³ Faculty of Electrical Engineering, Mechanical Engineering and Naval Architecture, University of Split, Split, Croatia

³⁴ Faculty of Engineering and Science, Western Norway University of Applied Sciences, Bergen, Norway

³⁵ Faculty of Nuclear Sciences and Physical Engineering, Czech Technical University in Prague, Prague, Czech Republic

- ³⁶ Faculty of Physics, Sofia University, Sofia, Bulgaria
³⁷ Faculty of Science, P.J. Šafárik University, Košice, Slovak Republic
³⁸ Frankfurt Institute for Advanced Studies, Johann Wolfgang Goethe-Universität Frankfurt, Frankfurt, Germany
³⁹ Fudan University, Shanghai, China
⁴⁰ Gangneung-Wonju National University, Gangneung, Republic of Korea
⁴¹ Gauhati University, Department of Physics, Guwahati, India
⁴² Helmholtz-Institut für Strahlen- und Kernphysik, Rheinische Friedrich-Wilhelms-Universität Bonn, Bonn, Germany
⁴³ Helsinki Institute of Physics (HIP), Helsinki, Finland
⁴⁴ High Energy Physics Group, Universidad Autónoma de Puebla, Puebla, Mexico
⁴⁵ Horia Hulubei National Institute of Physics and Nuclear Engineering, Bucharest, Romania
⁴⁶ HUN-REN Wigner Research Centre for Physics, Budapest, Hungary
⁴⁷ Indian Institute of Technology Bombay (IIT), Mumbai, India
⁴⁸ Indian Institute of Technology Indore, Indore, India
⁴⁹ INFN, Laboratori Nazionali di Frascati, Frascati, Italy
⁵⁰ INFN, Sezione di Bari, Bari, Italy
⁵¹ INFN, Sezione di Bologna, Bologna, Italy
⁵² INFN, Sezione di Cagliari, Cagliari, Italy
⁵³ INFN, Sezione di Catania, Catania, Italy
⁵⁴ INFN, Sezione di Padova, Padova, Italy
⁵⁵ INFN, Sezione di Pavia, Pavia, Italy
⁵⁶ INFN, Sezione di Torino, Turin, Italy
⁵⁷ INFN, Sezione di Trieste, Trieste, Italy
⁵⁸ Inha University, Incheon, Republic of Korea
⁵⁹ Institute for Gravitational and Subatomic Physics (GRASP), Utrecht University/Nikhef, Utrecht, Netherlands
⁶⁰ Institute of Experimental Physics, Slovak Academy of Sciences, Košice, Slovak Republic
⁶¹ Institute of Physics, Homi Bhabha National Institute, Bhubaneswar, India
⁶² Institute of Physics of the Czech Academy of Sciences, Prague, Czech Republic
⁶³ Institute of Space Science (ISS), Bucharest, Romania
⁶⁴ Institut für Kernphysik, Johann Wolfgang Goethe-Universität Frankfurt, Frankfurt, Germany
⁶⁵ Instituto de Ciencias Nucleares, Universidad Nacional Autónoma de México, Mexico City, Mexico
⁶⁶ Instituto de Física, Universidade Federal do Rio Grande do Sul (UFRGS), Porto Alegre, Brazil
⁶⁷ Instituto de Física, Universidad Nacional Autónoma de México, Mexico City, Mexico
⁶⁸ iThemba LABS, National Research Foundation, Somerset West, South Africa
⁶⁹ Jeonbuk National University, Jeonju, Republic of Korea
⁷⁰ Johann-Wolfgang-Goethe Universität Frankfurt Institut für Informatik, Fachbereich Informatik und Mathematik, Frankfurt, Germany
⁷¹ Korea Institute of Science and Technology Information, Daejeon, Republic of Korea
⁷² KTO Karatay University, Konya, Turkey
⁷³ Laboratoire de Physique Subatomique et de Cosmologie, Université Grenoble-Alpes, CNRS-IN2P3, Grenoble, France
⁷⁴ Lawrence Berkeley National Laboratory, Berkeley, California, United States
⁷⁵ Lund University Department of Physics, Division of Particle Physics, Lund, Sweden
⁷⁶ Nagasaki Institute of Applied Science, Nagasaki, Japan
⁷⁷ Nara Women's University (NWU), Nara, Japan
⁷⁸ National and Kapodistrian University of Athens, School of Science, Department of Physics , Athens, Greece
⁷⁹ National Centre for Nuclear Research, Warsaw, Poland
⁸⁰ National Institute of Science Education and Research, Homi Bhabha National Institute, Jatni, India
⁸¹ National Nuclear Research Center, Baku, Azerbaijan
⁸² National Research and Innovation Agency - BRIN, Jakarta, Indonesia
⁸³ Niels Bohr Institute, University of Copenhagen, Copenhagen, Denmark
⁸⁴ Nikhef, National institute for subatomic physics, Amsterdam, Netherlands
⁸⁵ Nuclear Physics Group, STFC Daresbury Laboratory, Daresbury, United Kingdom
⁸⁶ Nuclear Physics Institute of the Czech Academy of Sciences, Husinec-Řež, Czech Republic
⁸⁷ Oak Ridge National Laboratory, Oak Ridge, Tennessee, United States
⁸⁸ Ohio State University, Columbus, Ohio, United States

- ⁸⁹ Physics department, Faculty of science, University of Zagreb, Zagreb, Croatia
⁹⁰ Physics Department, Panjab University, Chandigarh, India
⁹¹ Physics Department, University of Jammu, Jammu, India
⁹² Physics Program and International Institute for Sustainability with Knotted Chiral Meta Matter (SKCM2), Hiroshima University, Hiroshima, Japan
⁹³ Physikalisches Institut, Eberhard-Karls-Universität Tübingen, Tübingen, Germany
⁹⁴ Physikalisches Institut, Ruprecht-Karls-Universität Heidelberg, Heidelberg, Germany
⁹⁵ Physik Department, Technische Universität München, Munich, Germany
⁹⁶ Politecnico di Bari and Sezione INFN, Bari, Italy
⁹⁷ Research Division and ExtreMe Matter Institute EMMI, GSI Helmholtzzentrum für Schwerionenforschung GmbH, Darmstadt, Germany
⁹⁸ Saga University, Saga, Japan
⁹⁹ Saha Institute of Nuclear Physics, Homi Bhabha National Institute, Kolkata, India
¹⁰⁰ School of Physics and Astronomy, University of Birmingham, Birmingham, United Kingdom
¹⁰¹ Sección Física, Departamento de Ciencias, Pontificia Universidad Católica del Perú, Lima, Peru
¹⁰² Stefan Meyer Institut für Subatomare Physik (SMI), Vienna, Austria
¹⁰³ SUBATECH, IMT Atlantique, Nantes Université, CNRS-IN2P3, Nantes, France
¹⁰⁴ Sungkyunkwan University, Suwon City, Republic of Korea
¹⁰⁵ Suranaree University of Technology, Nakhon Ratchasima, Thailand
¹⁰⁶ Technical University of Košice, Košice, Slovak Republic
¹⁰⁷ The Henryk Niewodniczanski Institute of Nuclear Physics, Polish Academy of Sciences, Cracow, Poland
¹⁰⁸ The University of Texas at Austin, Austin, Texas, United States
¹⁰⁹ Universidad Autónoma de Sinaloa, Culiacán, Mexico
¹¹⁰ Universidade de São Paulo (USP), São Paulo, Brazil
¹¹¹ Universidade Estadual de Campinas (UNICAMP), Campinas, Brazil
¹¹² Universidade Federal do ABC, Santo Andre, Brazil
¹¹³ Universitatea Națională de Știință și Tehnologie Politehnica Bucuresti, Bucharest, Romania
¹¹⁴ University of Cape Town, Cape Town, South Africa
¹¹⁵ University of Houston, Houston, Texas, United States
¹¹⁶ University of Jyväskylä, Jyväskylä, Finland
¹¹⁷ University of Kansas, Lawrence, Kansas, United States
¹¹⁸ University of Liverpool, Liverpool, United Kingdom
¹¹⁹ University of Science and Technology of China, Hefei, China
¹²⁰ University of South-Eastern Norway, Kongsberg, Norway
¹²¹ University of Tennessee, Knoxville, Tennessee, United States
¹²² University of the Witwatersrand, Johannesburg, South Africa
¹²³ University of Tokyo, Tokyo, Japan
¹²⁴ University of Tsukuba, Tsukuba, Japan
¹²⁵ Universität Münster, Institut für Kernphysik, Münster, Germany
¹²⁶ Université Clermont Auvergne, CNRS/IN2P3, LPC, Clermont-Ferrand, France
¹²⁷ Université de Lyon, CNRS/IN2P3, Institut de Physique des 2 Infinis de Lyon, Lyon, France
¹²⁸ Université de Strasbourg, CNRS, IPHC UMR 7178, F-67000 Strasbourg, France, Strasbourg, France
¹²⁹ Université Paris-Saclay, Centre d'Etudes de Saclay (CEA), IRFU, Département de Physique Nucléaire (DPhN), Saclay, France
¹³⁰ Université Paris-Saclay, CNRS/IN2P3, IJCLab, Orsay, France
¹³¹ Università degli Studi di Foggia, Foggia, Italy
¹³² Università del Piemonte Orientale, Vercelli, Italy
¹³³ Università di Brescia, Brescia, Italy
¹³⁴ Variable Energy Cyclotron Centre, Homi Bhabha National Institute, Kolkata, India
¹³⁵ Warsaw University of Technology, Warsaw, Poland
¹³⁶ Wayne State University, Detroit, Michigan, United States
¹³⁷ Yale University, New Haven, Connecticut, United States
¹³⁸ Yonsei University, Seoul, Republic of Korea
¹³⁹ Zentrum für Technologie und Transfer (ZTT), Worms, Germany
¹⁴⁰ Affiliated with an institute covered by a cooperation agreement with CERN
¹⁴¹ Affiliated with an international laboratory covered by a cooperation agreement with CERN.